RESEARCH ARTICLE

The Intersection of the Extrinsic Hedgehog and WNT/Wingless Signals with the Intrinsic Hox Code Underpins Branching Pattern and Tube Shape Diversity in the *Drosophila* Airways

Ryo Matsuda[1], Chie Hosono[1], Kaoru Saigo[2], Christos Samakovlis[1,3] *

1 Department of Molecular Biosciences, The Wenner-Gren Institute, Stockholm University, Stockholm, Sweden, 2 Department of Biophysics and Biochemistry, Graduate School of Science, University of Tokyo, Tokyo, Japan, 3 ECCPS, University of Giessen, Giessen, Germany

* christos.samakovlis@su.se

Abstract

The tubular networks of the *Drosophila* respiratory system and our vasculature show distinct branching patterns and tube shapes in different body regions. These local variations are crucial for organ function and organismal fitness. Organotypic patterns and tube geometries in branched networks are typically controlled by variations of extrinsic signaling but the impact of intrinsic factors on branch patterns and shapes is not well explored. Here, we show that the intersection of extrinsic *hedgehog*(*hh*) and *WNT/wingless* (*wg*) signaling with the tube-intrinsic Hox code of distinct segments specifies the tube pattern and shape of the *Drosophila* airways. In the cephalic part of the airways, *hh* signaling induces expression of the transcription factor (TF) *knirps* (*kni*) in the anterior dorsal trunk (DTa1). *kni* represses the expression of another TF *spalt major* (*salm*), making DTa1 a narrow and long tube. In DTa branches of more posterior metameres, Bithorax Complex (BX-C) Hox genes autonomously divert *hh* signaling from inducing *kni*, thereby allowing DTa branches to develop as *salm*-dependent thick and short tubes. Moreover, the differential expression of BX-C genes is partly responsible for the anterior-to-posterior gradual increase of the DT tube diameter through regulating the expression level of Salm, a transcriptional target of *WNT/wg* signaling. Thus, our results highlight how tube intrinsic differential competence can diversify tube morphology without changing availabilities of extrinsic factors.

Author Summary

Tubes are common structural elements of many internal organs, facilitating fluid flow and material exchange. To meet the local needs of diverse tissues, the branching patterns and tube shapes vary regionally. Diametric tapering and specialized branch targeting to the

brain represent two common examples of variations with organismal benefits in the *Drosophila* airways and our vascular system. Several extrinsic signals instruct tube diversifications but the impact of intrinsic factors remains underexplored. Here, we show that the local, tube-intrinsic Hox code instructs the pattern and shape of the dorsal trunk (DT), the main *Drosophila* airway. In the cephalic part (DT1), where Bithorax Complex (BX-C) Hox genes are not expressed, the extrinsic Hedgehog signal is epistatic to WNT/Wingless signals. Hedgehog instructs anterior DT1 cells to take a long and narrow tube fate targeting the brain. In more posterior metameres, BX-C genes make the extrinsic WNT/Wingless signals epistatic over Hedgehog. There, WNT/Wingless instruct all DT cells to take the thick and short tube fate. Moreover, BX-C genes modulate the outputs of *WNT/wingless* signaling, making the DT tubes thicker in more posterior metameres. We provide a model for how intrinsic factors modify extrinsic signaling to control regional tube morphologies in a network.

Introduction

Branched tubular networks, like our vasculature transport and exchange vital gases and nutrients along entire organisms. The branching patterns, tube structures and dimensions in these networks show considerable regional variations to meet the different needs of target organs and ensure optimal organ function and animal fitness [1–4]. Adaptations of branch morphologies to the tissue environments can be achieved by changing the local availability of extrinsic factors like guidance molecules and/or by intrinsic regional differences in tube cell competence to respond and modify signaling outcomes. Although the prominent roles of variations in extrinsic signals in organotypic branching become widely established [3,5,6], the tube intrinsic mechanisms determining the differential responses of tube cells to signaling remain to be explored [7–10].

Despite the huge evolutionary distance of insects and mammals, the formation and maturation of the respiratory tube network in *Drosophila melanogaster* has served as a fruitful model system of branching morphogenesis [11,12]. Here, we use this system to evaluate the contribution of tube intrinsic, regionally differential competence in diversification of tube morphology.

The fly respiratory network, also called the tracheal system ramifies extensively to deliver oxygen to each cell in the body (Fig. 1A) [13,14]. It derives from 10 primordial cell clusters specified in ectodermal para-segments (PS) 4–13 on each side of the body [15]. At stage 11, the metameric cell clusters invaginate and begin to extend 6 primary branches. The tracheal metameres (Tr1-10) interconnect into a network through the activities of 5 to 6 specialized fusion cells in each branching unit [16–18]. These cells find and adhere to their ipsilateral or contralateral counterparts in neighboring metameres to form continuous tubes.

Tracheal branching morphogenesis is controlled by two conceptually different groups of extrinsic signals [6,19]. One is required in all primary branches while the other class specifies unique sets of primary branches. FGF/Branchless (Bnl) [20] is dynamically expressed in the surrounding tissues and serves as a general extrinsic branching signal by activating FGFR/Breathless (Btl) on the airway cells [21–23]. Btl activation initiates oriented cell migration and enhances branch elongation while it also organizes cell fate specification along each primary branch. The gradual specification of distinct fusion and terminal cell fates at the branch tips is essential for both branch fusion and further ramification branching [14,20].

The second class of signals includes BMP, Wnts and Hh proteins. BMP/Decapentaplegic (Dpp) is expressed in dorsal and lateral stripes along the length of the embryo [24]. Dpp
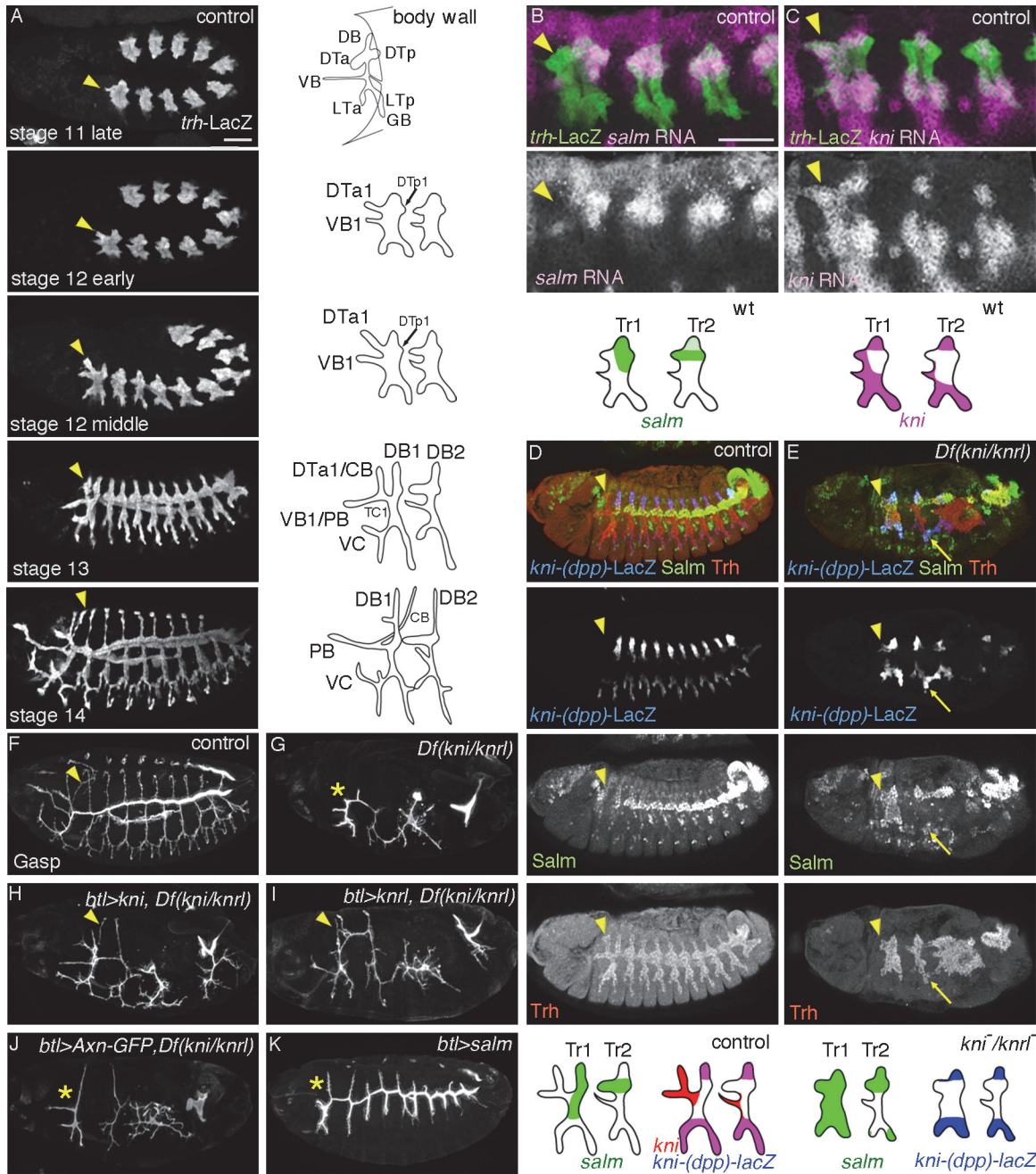
Figure 1. Developmental and genetic distinction between DTa1 and the rest of DT. Embryos are aligned with their anterior left and dorsal up unless otherwise indicated. (A), Times series of airway development visualized with *trh-lacZ*. DTa1 is marked with arrowheads. Schemes of the typical primary branches or the metamere 1/2 are shown on the right. See text for details. (B, C), Late stage11 embryos marked with *trh*-LacZ and RNA *in situ* hybridization against *salm* (B) or *kni* (C). Typically, DT and DB initiate *salm* expression while *kni* expression represses *salm* later in the DB. Note that DTa1 (arrowheads) expresses *kni* but not *salm*.(D, E) Stage 13 control and *Df(kni/knrl)* embryos marked with *kni-(dpp)*-LacZ, Salm and Trh. Schemes of their expression are shown in the bottom. In the control (D), Salm is detected in DTp1-DT10. Salm is also reproducibly detected in DB1/10 and TC1. *kni-(dpp)*-LacZ marks subsets of Kni positive branches (DB/TC/GB) responding to *dpp* signaling. *kni-(dpp)*-LacZ and Salm overlap only in DB1/10. In *Df(kni/knrl)* (E), some abdominal segments are missing or fused. Note that *kni-(dpp)*-LacZ positive cells co-express Salm in DB, LT or GB (arrow) and that the whole terminal metameres, presumably Tr1/10, including DTa1 (arrowhead) express Salm. (F-K) Airway branching revealed by Gasp expression at stage 15. DTa1/CB is marked with arrowheads or asterisks. Compared to the control (F), in *Df(kni/knrl)* (G), *kni* positive branches (DB, LT, GB, VB and DTa1) are stalled or missing. Branches in Tr1 and Tr10 become very thick. *btl-gal4* driven *UAS-kni* (H) or *UAS-knrl* (I) significantly recues DTa1/CB formation. *btl-gal4* driven *UAS-Axn-GFP* (J) partially rescues DB extension without effects on dorsalward extension of CB while *btl-gal4* driven *UAS-salm* abrogates CB formation (K). Scales bars: 50um.

doi:10.1371/journal.pgen.1004929.g001

signaling specifies and licenses dorsally (dorsal branch, DB) and ventrally migrating primary branches (lateral trunk, LT and ganglionic branch, GB) by inducing the expression of the TFs *kni* and *knirps-related* (*knrl*) in airway cells [24–26]. Wg is expressed in a repetitive pattern of transverse ectodermal stripes and together with other WNT signaling molecules specifies dorsal trunk (DT) identity [27–29]. It upregulates the expression of the TF *salm* [30] in the major airways of the network. *salm* promotes short and thick tubes by suppressing intercalation of the tube constituent cells [31,32]. On the other hand, *kni/knrl* can repress *salm* expression in DB [25] and promotes cell intercalation in the long and narrow tubes of dorsal (DB) and ventral branches [31]. Hh is also segmentally expressed in ectodermal stripes and modulates the airway branching, both indirectly through positive regulation of *bnl* expression [33] and directly by acting on terminal cell specification or extension [34,35]. The functions of *hh* in primary branching remain to be thoroughly studied [34,36,37]. Collectively, the differential primary branch identities established by the second class of extrinsic signals are intimately linked with the distinctive branching patterns and dimensions of individual primary branches [38].

The region-specific modification of serially homologous organs and appendices is a general theme in animal development [39–42]. The evolutionary conserved Hox gene complexes are key selector genes of tissue identities along the anterior posterior (A-P) axis of animals [39,41,43–45] [46–50]. In *Drosophila*, 2 groups of Hox genes, the Antennapedia complex (ANTP-C) and Bithorax complex (BX-C) confer regional differences to the body plan by graded expression of their products in register with para-segmental units [39,51]. The 3 protein-coding genes of the BX-C [52] are expressed in distinct and partially overlapping domains along the A-P embryonic axis. *Ultrabithorax* (*Ubx*) expression initiates in the cells of PS5, *abdominal-A* (*abdA*) expression starts from PS7 and *Abdominal-B* (*AbdB*) from PS10 [44,53]. A connection between regional modification of airway morphology and Hox genes has been established already in the early studies of Hox-gene mutants. Upon loss of all BX-C genes the tracheal metameres Tr2-Tr10 become transformed to Tr1 [39,54]. However, the genetic and molecular mechanisms establishing the different branch morphologies along the airway tubes have been largely unexplored.

Here, we focus on the regulation of 2 distinct morphological modifications along the DT major airways. We first analyze how the most anterior part of the DT diverges its branching pattern and tube size to generate long and narrow tubes targeting the head. We show that these regional modifications in cell behaviors are controlled by a combination of *hh* signaling and the airway intrinsic Hox code. We further investigate the mechanism of tube tapering in the central domain of the DT airways. We find that BX-C genes modulate the anterior-to-posterior gradation of DT tube diameter partly through regulating the expression of level of *salm*, a target of *WNT/wg* signaling. Our work highlights that the intrinsic Hox code locally modifies the outcomes of extrinsic signals to establish regionally different branching patterns and to coordinate tube shapes in register with the embryo axis.

Results and Discussion

Specialized branching patterns and tube shapes in Tr1

The DT is a continuous tube running along the A-P axis of the embryo. It connects with the exterior through the narrow tube of the spiracular chamber in the posterior spiracle (PSP) [55]. The DT is constructed by the fusion of an anterior (DTa) and a posterior (DTp) branch from each tracheal metamere (Tr1-Tr10) [13,17]. The DT airway encompasses several regional variations that provide a suitable system for the study of the interplay of external signaling with intrinsic factors during tube morphogenesis [13]. First, the most anterior end of the DT extends several specialized branches (see below). Second, it shows a pronounced posterior to anterior

diameter tapering contrasting the largely cylindrical shape of other primary branches in the network. Third, its most anterior metameric unit (Tr1) lacks a DTa fusion cell, whereas the most posterior one (Tr10) does not generate a fusion cell in its posterior branch (DTp).

More generally, Tr1 is distinct from the rest of the tracheal metameres because it encompasses more cells and branches to oxygenate the specialized organs of the head and thorax. The specialized branches of Tr1 include the cerebral branch (CB) targeting the brain, the pharyngeal branch (PB) to the anterior intestine, the ventral cephalic branch (VC) extending to epidermis and muscles and the ganglionic branch GB0, which penetrates the ventral nerve cord. Among these, the CB and VC are directly linked to the anterior end of the DT airways.

Despite the pronounced differences in the final branching patterns, branching in Tr1 is comparable to the common stereotypic primary branching of Tr2-Tr9 during stage 11 (Fig. 1A). At stage 12 however, DTa1, elongates further than other DTa branches and shifts dorsally. By stage 13, visceral branch 1 (VB1) and DTa1 co-segregate from the transverse connectives (TC). Later, DTa1 extends dorsally and posteriorly and turns towards the brain, forming CB [13]. DTa1/CB develops very narrow and long tubes compared to the thick and short DT branches in posterior metameres. VB1 extends more anteriorly, forming the pharyngeal branch (PB) (Fig. 1A).

kni expression in DTa1/CB is essential for CB formation

The gradual morphological diversification of CB/DTa1 compared to DTa braches in other metameres prompted us to examine the expression of branch identity TFs, *salm* and *kni*. In a "typical", central metamere, *salm* expression is upregulated by *wg/WNT* signaling [27–29] and is detected in DB and DT at stage 11 [30]. Later, *kni* is induced in DBs by *dpp*, where it represses *salm* expression [24–26]. *kni and salm* are co-expressed in DB1/10 (see below). In contrast to the DTa of other metameres, we found that *kni* expression is strongly upregulated in DTa1 from late stage 11 (Fig. 1B). Concomitantly, *salm* is not detectable in DTa1 (Fig. 1C) although it becomes upregulated in DTp1 as in other metameres (Fig. 1D) [30].

To test the significance of the differential *kni* expression in DTa1 we analyzed mutants lacking both *kni* and its paralog *knrl*. In these chromosomal deficiency mutants, the abdominal segments are missing due to the early gap gene function of *kni*, while trunk development is rather normal [56]. In the trunk region of *Df(kni/knrl)* mutants, the formation of *kni* positive primary branches [24,25] is variably affected, ranging from complete absence to branch stalling [25], while the *salm*-positive DT branches can form and fuse (see below) [57]. We noticed that in *kni/knrl* mutants, airway cells initiate branch outgrowth in the dorsal and ventral directions and respond to *dpp* by inducing the *dpp*-responsive kni reporter, *kni-(dpp)-lacZ* (Fig. 1E). In these embryos, *salm* is ectopically detected in *kni-(dpp)-lacZ* positive cells in either dorsal or ventral cells near the *wg* stripe (Fig. 1E). This suggests that *dpp* mediated *kni/knrl* induction suppresses *salm* induction by *wg* in both the dorsal [25,26] and ventral branches. However, in the first and the last metameres of *Df(kni/knrl)* mutants, *salm* expression additionally expands to nearly cover the entire metamere, including the putative CB/DTa1 (Fig. 1E). This suggests that *kni* functions in DTa1 to repress *salm*. Additionally, the competence of tracheal cells to induce *salm* is differentially modulated in the terminal Tr1 and Tr10 metameres compared to the central metameres.

Consistent with the notion that generalized reduction of *wg/WNT* signaling can bypass the requirement of *dpp/BMP* signaling during DB extension in Tr2-Tr10 [31], *btl*-Gal4 [58] mediated overexpression of GFP fused to Axin (Axn) [59–61], a negative regulator of *wg* signaling moderately rescues dorsal extension of the residual DBs (DB1 and DB2) of *Df(kni/knrl)* mutants but does not appreciably rescue the extension of DTa1/CB (Fig. 1J). In sharp contrast, *btl-*

gal4 driven *UAS-kni* or *UAS-knrl* in *Df(kni/knrl)* mutants restores CB formation ([Fig. 1F-I](#)). Thus, we conclude that *kni* induction and the resultant *salm* repression in DTa1/CB are essential for its formation and extension. In support for this, *btl-gal4* driven *UAS-salm* in wild-type background significantly suppresses DTa1/CB formation but has little effect on the extension of DTa in Tr2-Tr10 [28,62], which endogenously expresses *salm* ([Fig. 1K](#)). Collectively, the results suggest that *kni* induction and the resultant *salm* repression in DTa1/CB are essential for its formation and extension.

hh is necessary for DTa1 patterning

The diversified expression of *kni* in DTa1 compared to the remaining DTa branches could be regulated by differential expression of exogenous guidance factors around DTa1 and/or by intrinsic differences of competence among the DT1 cells. Firstly, to investigate which extrinsic factors are upstream of *kni* induction in DTa1, we analyzed the expression or function of known, secreted airway branching regulators.

At stage 11, Tr1 like the rest of the tracheal metameres is surrounded by 6 patches of *bnl* expressing cells, prefiguring the stereotypic directions of the common primary branches ([S1A Fig.](#)). This general pattern diversifies in the cephalic region of stage 12 embryos, where the DTa1 migrates toward a more dorsal *bnl* expression spot ([S1B Fig.](#)). Despite this difference, *kni* induction in DTa1 is still detected in *btl* mutants ([S1C,D Fig.](#)), excluding a major role of *bnl* in *kni* induction in DTa1. *dEGFR/faint little ball/torpedo (top)* [63] encodes an RTK that is suggested to positively act on *salm* expression [64] upon binding the Spitz/EGF ligand [65]. In embryos mutant for *rhomboid (rho)*, encoding a protease required for generating the active Spitz [66,67] or for *dEGFR*, the expression of *kni* in the DTa1/CB still occurs ([S1E,F Fig.](#)). This argues against a role of localized dEGFR activation in controling *kni* expression in DTa1.

dpp and *wg* are known inducers of *kni/knrl* in DB [24] and *salm* in DT [27,28], respectively, in a "typical" metamere. Thus, variations of their expression in the Tr1 proximity might influence the specialized expression patterns of *kni* or *salm* in DTa1. However, the expression of both *dpp* and *wg* is comparable around Tr1-3 ([S1G, H Fig.](#)), arguing against an instructive role of these two factors in *kni* induction in DTa1. Indeed, neither mutants of *tkv*, encoding one of the two *dpp* receptor subunits [68,69] nor *arm* mutants lacking an essential component of *wg* signaling [70–72], showed major defects in *kni* induction and outgrowth of DTa1/CB ([S1I, J Fig.](#)).

hh is a signaling molecule that binds its receptor *patched* (*ptc*), thereby relieving *ptc*-mediated inhibition of the 7 transmembrane domain protein *smoothened* (*smo*) [73,74]. *hh* is expressed in stripes in the ectoderm, abutting the anterior edge of the airway primordia at stage 10 and overlying the anterior part of the invaginated airway cells of each metamere at stage 11 ([S1K, L Fig.](#)) [34]. Glazer and Shilo showed that *hh* induces marker gene expression in the anteriorly migrating branches of central metameres [34], arguing that *hh* signaling patterns the anterior primary branch fates of the "typical", central metameres. We found that just after invagination of the airway primordial cells, expression of *ptc*, a transcriptional target of *hh* [75,76] is upregulated in the DTa1 precursors ([Fig. 2A](#)), suggesting that *hh* signaling is active there. In *hh* mutants the dorsalward CB extension is hardly detectable and *salm* expression is expanded in the entire DT1 ([Fig. 2B-D](#)). This suggests that *hh* signaling in DTa1 induces *kni* and thereby represses *salm* expression. Among the ectopically *salm* expressing cells in DTa1, some cells also express *kni* while others do not. We suggest that in the absence of *hh* signaling, *hh* responsive *kni* induction is lost while *dpp* signaling may take over to induce *kni* expression in some *salm* positive cells. Such an ectopic activation of *kni* in the absence of *hh* could induce ectopic *kni/salm*-double positive cells resembling DB1 cells. This interpretation is consistent with the
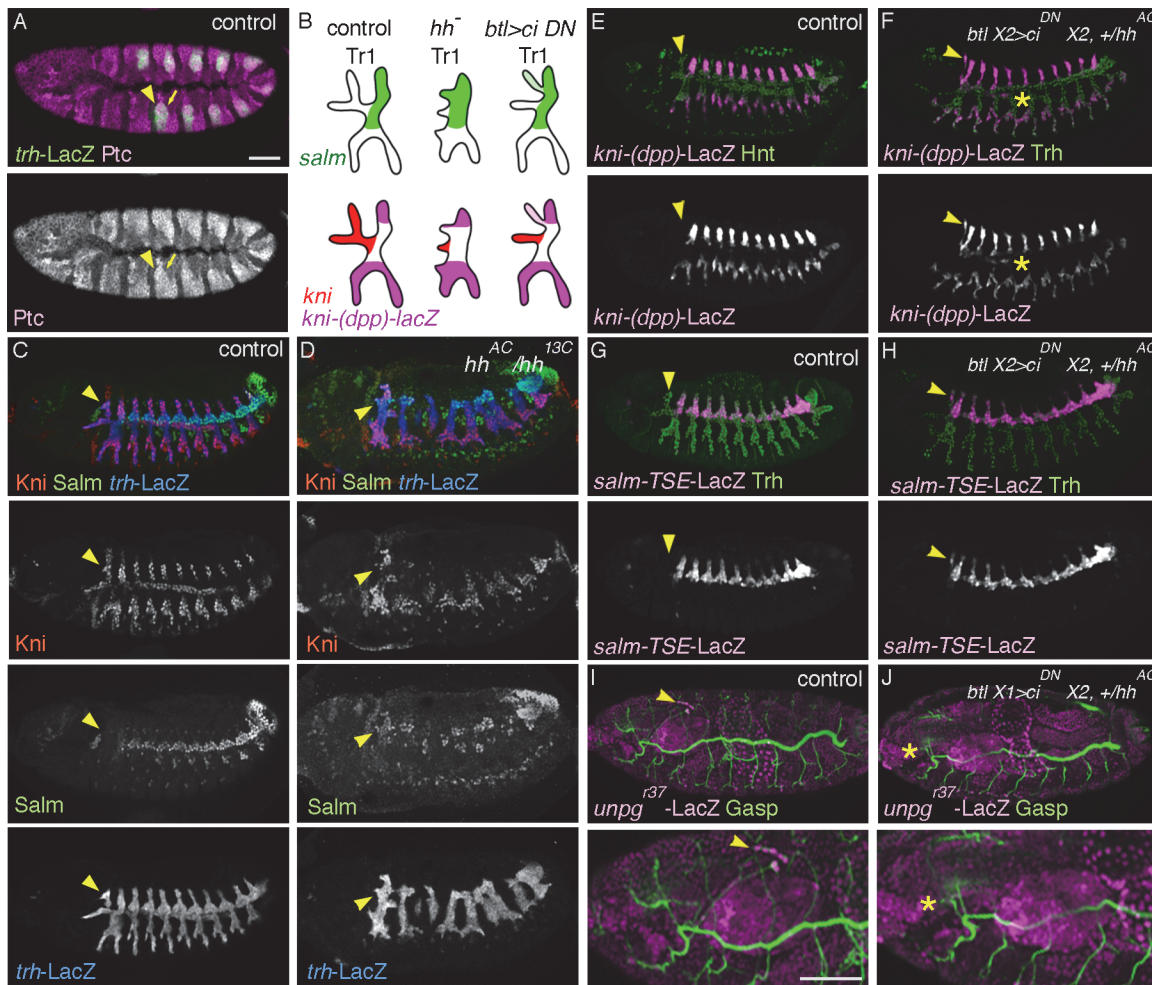
Figure 2. hh signaling in the airways is required for DTa1 development. (A) At stage 11, Ptc is detected strongly in all of the invaginated airway primodia (arrow) marked with *trh*-LacZ, with the strongest expression in the anterior part (arrowhead). (B-J) Effects of loss of *hh* signaling on DTa1 development. Arrowheads mark DTa1. A summary of phenotypes is shown in (B). (C, D) Expression of Kni and Salm at stage 13 in relation to the airway development visualized with *trh*-LacZ. In the control (C), DTa1 expresses Kni but not Salm while in *hh* mutants (D) the DTa1 remnant often expresses Salm. Kni is variably detected in these DTa1 remnants. (E-J) Effects of *btl-gal4* mediated overexpression of *ci^{DN}* on expression of *kni-(dpp)-lacZ* and *salm-TSE-lacZ*. The airway cells are labeled by Trh or Hindsight (Hnt) [126]. In the control (E,G), *kni-(dpp)*-LacZ (E) is detected in DB, LT and GB while *salm-TSE*-LacZ (G) is detected in DT except for DTa1. Upon overexpression of Ci^{DN} with *btl*-Gal4 (F, H), DTa1/CB additionally becomes positive for respective enhancer reporters. Asterisks mark *kni-(dpp)*-LacZ expression ectopically induced in VB. (I, J) Stage 16 embryos marked with Gasp and *unpg*-LacZ. Parts of each image are enlarged in the bottom. In the control (I), CB forms a slightly thinner branch compared to DB1 and its tips strongly express *unpg*-LacZ. Overexpression of Ci^{DN} variably generates CBs resembling DB1 in branching patterns, tube diameter or lack of *unpg*-LacZ expression (J). Asterisk marks the misrouted CB/DTa1. Scales bars: 50um.

doi:10.1371/journal.pgen.1004929.g002

de-repression of *kni-(dpp)-lacZ* in *Df(kni/knrl)* mutants (Fig. 1E). Thus, we conclude that *hh* signaling is required to induce *kni* and to repress *salm* in DTa1. The earlier function of *hh* is also required for the maintenance of the striped expression of *wg* [75,77], which induces *salm* expression in DT. Thus, the variability of *salm* expression either in DTa1 or in DTa/DTp of any metamere in *hh* mutants may partly reflect a reduction or loss of epidermal *wg* expression.

In *hh* mutants, *bnl* expression guiding DB migration in central metameres is lost but *bnl* expression in surrounding cells guiding CB is still detectable at stage 12 (S1M Fig.). Nevertheless, the dorsal extension of a CB-like branch is not detected in *hh* mutants at later stages (S1N Fig.). To more directly address the effect of *hh* signaling in DTa1 we attempted to inactivate its components specifically in the airways. *hh* signaling modifies the transcriptional activity of *cubitus*

interruptus (*ci*) [74]. In the absence of *hh*, Ci is proteolytically processed and acts as a repressor [78], while upon *hh* pathway activation, *smo* mediated signaling suppresses this proteolysis and turns Ci into an activator [78–80]. The balance of loss of the repressor form and generation of the activator form of Ci determines the *hh* signaling outputs [79–81]. We generated embryos expressing dominant negative forms of *ci*, *ci*^{DN} (*ci*^{rep} [82,83] and/or *ci*^{75} [78,84]) exclusively in the airways and assessed the expression levels of *kni-(dpp)-lacZ* (a DB and LT/GB marker) [25] and of *salm-TSE-lacZ* (a reporter of *salm* expression) [30] in metamere 1. Both markers are ectopically induced in the DTa1 of these embryos at stage 13 (Fig. 2E-H) although the cell number in this branch did not significantly change (20 cells, standard deviation SD = 0.707 for 5 wild type embryos at stage 13 and 19.2 cells, SD = 0.447 for 5 *btl*X2> *ci*^{rep} embryos). We interpret that the incomplete inactivation of *hh* signaling in the airways by *ci*^{DN}, partially transformed DTa1 cells to DTp1. These cells are still receiving enough Dpp to express *kni-(dpp)-lacZ*. The weaker effects of *ci*^{DN} expressing embryos compared to *hh* mutants may reflect ineffectiveness of Ci^{DN} or the delayed *btl*-Gal4 mediated expression [58] of Ci^{DN}, which starts slightly later than the initiation of *hh* action on DTa1. Additionally, the airway-specific overexpression of Ci^{DN} or general *hh* inactivation in *smo* mutants frequently resulted in DTa1/VB1 co-segregation defects and CB misrouting at stage 16 (Fig. 2I, J and S1O Fig.). A similar CB misrouting phenotype has been described in mutants of *unplugged* (*unpg*) encoding a TF expressed in CB [54]. Indeed, the expression of an *unpg* enhancer trap in the CB of wild type embryos is lost upon Ci^{DN} overexpression (Fig. 2I, J).

Collectively, these results identify a selective, direct role of *hh* signaling in inducing the distinct cell identities of DTa1 compared to the cells of the remaining DT branches.

hh pathway overactivation transforms DB1 and DTp1 into DTa1-like branches

The transformation of DTa1 to DTp1/DB1 upon inhibition of *hh* signaling suggests that its overactivation may be sufficient to transform DTp1/DB1 to DTa1. To examine this, we analyzed *ptc* mutants, where *hh* signaling is inappropriately activated due to the loss of *ptc*-mediated inhibition of *smo* [73,74]. In *ptc* mutants, the dorsal part of metamere 1 expresses Kni but not Salm already at late stage 11 (Fig. 3A, B). Correspondingly at stage 13, expression of *salm-TSE-lacZ* is specifically lost from metamere 1, suggesting a defect in both DTp1 and DB1 specification (Fig. 3C and S3A Fig., note that in wild type, *salm* is expressed in DB1 and DTp1). Consistent with a loss of the DB1 fate in *ptc* mutants, *kni-(dpp)-lacZ* expression in the dorsal part of metamere 1 is completely lost (Fig. 3E) while Kni protein is expressed in the whole distal part of Tr1 (S2B Fig.). Although *ptc* mutants contain fewer airway cells [33], presumably due to an early upregulation of *wg* [85], a negative regulator of the airway primodia size [86], reduction of cell number in *CycA* mutants [38] does not significantly abrogate DB1/DT1 fates (S2D, H Fig.). This suggests that the effect of *ptc* on DB1/DT1 specification is more direct and not due to a general reduction in the number of airway cells. Because *btl*-Gal4 driven Ci^{rep} (Fig. 3D, F) or Ci^{75} can restore the expression of both *kni-(dpp)-lacZ* and *sal-TSE-lacZ* in the Tr1 cells of *ptc* mutants and because Ptc is expressed in all airway primordia including the entire Tr1 primordium (Fig. 2A), these results suggest that overactivation of *hh* signaling in Tr1 abolishes the DTp1/DB1 fates.

To further test the role of *hh* signaling in determining branch identities in Tr1 we analyzed the RNA expression of *unpg*. In control embryos at early stage 12, *unpg* expression is strongly detected in DTa1 [54] and weakly in the anterior part of TC1. Both of these regions correspond to *hh* signaling activation (Fig. 3G). At stage 13, *unpg* RNA is detected in CB and GB0/GB1 in Tr1 and also in the GBs of the more posterior metameres Tr2-Tr9 (Fig. 3H) [54]. Consistent
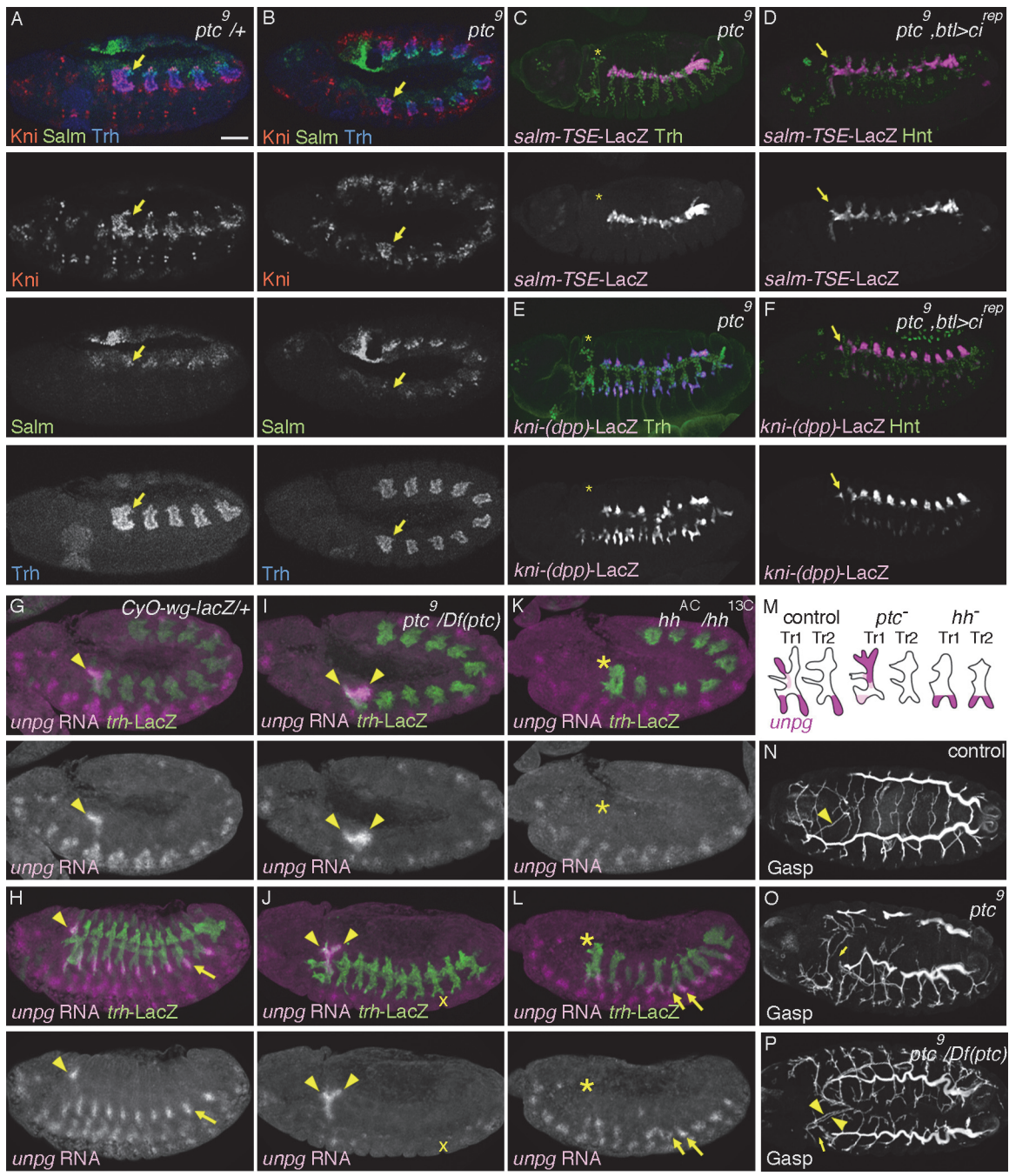
Figure 3. Overactivation of *hh* signaling transforms the primary branch identities in Tr1. (A, B) Expression of Salm, Kni and Trh at late stage 11. In contrast to the control (A), where Salm is upregulated in DTp1 (arrow), in *ptc* mutants (B), Salm upregulation in DTp1 (arrow) is not detected and Kni occupies the whole distal part of Tr1. Note that the airway primordia look smaller in *ptc* mutants [33]. (C-F) Effects of *ptc* mutations on *kni-(dpp)-lacZ* and *salm-TSE-lacZ* expression. The airway cells are labeled by Trh or Hnt. Compared to the control (Fig. 2E,G), in *ptc* mutants (C, E), the expression of *salm-TSE-lacZ* (C) and *kni-(dpp)-lacZ* (E) is lost from the dorsal part of Tr1 (asterisks). Overexpression of Ci^{DN} with *btl*-Gal4 in *ptc* mutants restores their expression in Tr1 (D, F, arrows). (G-M) *unpg* RNA expression at stage 12 (G, I, K) and stage 13 (H, J, L) in relation to the airway development visualized with *trh-lacZ*. A summary of phenotypes is shown in (M). (G, H) In the control, *unpg* RNA is strongly detected in CB (arrowheads) at stages 12 and 13. *unpg* expression is also strong in GB at stage 13 (arrow). (I, J) In *ptc* mutants, *unpg* expression is expanded to DB1, DTp1 and TC1 (arrowheads) while its expression in GB is barely detectable (asterisks). (K, L) In *hh* mutants, *unpg* expression is lost in CB (asterisk) while it is derepressed in LTa in the central metameres (arrows). (N-P) Airway branching pattern visualized by Gasp. Compared to the control (N), *ptc* mutants (O, P) show persistent loss of DT1/2 fusion (asterisks). In addition, duplication of CB like branches occasionally happen (P, arrowheads). Scales bars: 50um.

doi:10.1371/journal.pgen.1004929.g003

with the loss of *unpg-lacZ* expression in CB upon Ci^DN overexpression, *unpg* RNA expression is lost in DTa1/CB of *hh* mutants (Fig. 3K, L). Conversely in *ptc* mutants, it is expanded posteriorly to cover the positions of DB1/DTp1/TC1 (Fig. 3I, J), indicating their transformation to CB-like fates. Consistent with the expanded *unpg* expression, we often detected a duplication of CB-like branches in *ptc* mutants (Fig. 3P). We additionally noted that *unpg* expression in GB is lost in *ptc* mutants (Fig. 3J) while *unpg* is derepressed in LTa in *hh* mutants (Fig. 3L), in accord with the notion that *hh* confers the anterior branch identity in the central metameres [34].

At stage 16, *ptc* mutants show variable branching defects including stalled GBs, DBs and DT breaks [33]. Concomitantly with the loss of DTp1 fate marker (*salm-TSE-lacZ*), DT1 and DT2 never fuse in *ptc* mutants (Fig. 3N-P). In wild type, one of DTp1 cells takes the fusion cell fate, activates *dys* expression and attaches to a fusion cell in DTa2 (S2E Fig.), [18]. In *ptc* mutants, *dys* is not activated in DTp1 while *dys* expression is variably expanded in more cells of the DT branches in posterior metameres (S2E-G Fig.). This may reflect an increase of epidermal expression of *wg* [85], an inducer of the fusion cell fates [27,28]. The failure of *dys* activation and DT1 fusion in *ptc* mutants is significantly rescued by *btl*-Gal4 mediated overexpression of Ci^rep (S2I Fig.). Moreover, both loss of *dys* expression in DT1 as well as DT1/2 fusion defects are variably observed when dominant active Ci, Ci^act [84,87] is overexpressed in the airway cells (S2J Fig.). Notably however, the Ci^act overexpression by *btl*-Gal4 did not diminish *salm-TSE-lacZ* or *kni-(dpp)-lacZ* expression.

In summary, we suggest that *hh* signaling instructs the DTa1 fate at the expense of DB1/DTp1 fates. In DTp1, *hh* signaling must be kept low to allow the proper selection of the fusion cell fate and subsequent DT1/DT2 branch fusion.

Abdominal Hox genes shunt *hh* signaling from induction of *kni* in DTa

The *hh* induction of *kni* expression in the DTa of wild type embryos as well as the loss of DT/DB fates in *ptc* mutants are confined to Tr1. However, *hh* signaling outcomes are expected to be equally profound in the more posterior metameres of both wild type [34] and *ptc* mutant embryos [33]. The exclusive restriction of Hh responses within Tr1 implies the presence of an inhibitory mechanism preventing *kni* activation in the DTa branches of posterior metameres. The BX-C genes represent obvious candidate regulators of posterior metamere identity and modulators of *hh* signaling outcomes along the A-P axis of the airways. Indeed, *unpg* expression is de-repressed in progressively more posterior metameres in *Ubx* mutants and *Ubx abdA AbdB* triple mutants [54].

BX-C gene expression is graded along the A-P axis of the airway metameres (S3A-D Fig.). *Ubx* expression starts in Tr2 (PS5) and peaks at Tr3 (PS6) (S3A Fig.). *abdA* expression starts in Tr4 (PS7) and peaks in Tr6 (PS9) (S3B Fig.) while *AbdB* expression starts in Tr7 (PS10) and peaks in Tr10 (PS13) (S3C Fig.). These expression patterns are in register with the expression of BX-C genes in the ectoderm [53], which is the origin of the airway primordia.

To explore the function of BX-C genes in DTa fates, we first monitored *dys* expression in various BX-C mutants. In *Ubx* mutants, single fusion cells are detected in Tr1, Tr2 and Tr3 (S3E, F Fig.) suggesting that DTa2 and 3 are transformed to become DTa1/CB. *abdA* single mutants do not show *dys* expression defects in the DT (S3G Fig.) while a superfluous fusion cell in DTp10 is detected in both *AbdB* single and *abdA AbdB* double mutants (S3H, I Fig.). This suggests that DT10, which normally contains only a single fusion cell in its DTa branch, is transformed into a more anterior identity. Compared to *Ubx* single mutants, *Ubx abdA* double mutants have single fusion cells in Tr1–8 and often in Tr9 (S3J Fig.). In *Ubx abdA AbdB* triple mutants, the DT stumps of all metameres contain single fusion cells (S3K Fig.). This implies

that DTa branches in progressively more posterior metameres are transformed to become DTa1 upon progressive loss of BX-C genes [39]. Any single gene of the BX-C is sufficient to suppress the DTa1 fate. Consistently, we detected expansion of *kni* expression and a loss of *salm* in the transformed DTa in *Ubx* single, *Ubx abdA* double and *Ubx abdA AbdB* triple mutants (Fig. 4A-C). These phenotypes are often accompanied with the appearance of dorsally extending branches that are positive for Kni but negative for *kni-(dpp)*-LacZ, Salm and *salm-TSE*-LacZ, resembling the CBs of wild type embryos (S3K Fig.) [54]. The marker expression analysis in BX-C mutants suggests that in the posterior metameres, *Ubx, abdA* and *AbdB* interfere with the outcomes of *hh* signaling.

If the antagonistic role of BX-C on *hh*-mediated *kni* induction reflects an essential function of the BX-C in posterior metameres, one might expect some rescue of the branching defects of BX-C mutants upon simultaneous loss of *hh* or *kni/knrl*. Indeed, *salm* expression is de-repressed in DTa1-9 of *Ubx abdA hh* and of *Ubx abdA kni/knrl* mutants (Fig. 4D, E). Additionally, DT fusion is weakly restored in both the triple and quadruple mutants (S3L, M Fig.).

Taken together, we suggest that BX-C genes antagonize *hh*-mediated induction of *kni* in DTa branches.

Airway-specific expression of abdominal Hox genes diverts *hh* signaling from *kni* activation

In addition to the airways, BX-C genes are expressed in many embryonic tissues. Where do they act to divert *hh* signaling from *kni* induction in the DT branches? In lack of reagents for the reliable conditional inactivation of the BX-C genes in the airways, we monitored the effects of airway-specific ectopic expression of BX-C genes on DT1 cell specification. The first metamere does not express the BX-C genes (S3A-D Fig.) and thereby may provide a naïve environment for assessing the effects of their overexpression on marker gene activation [41]. *btl*-Gal4 mediated overexpression of any of the BX-C genes in wild type background, variably decreases *kni* expression in the DTa1 and concomitantly leads to increased *salm* levels at stage 13/14 (Fig. 4F-J). At later stages, DTa1 branches are thick, resembling typical DTa branches of posterior metameres (see below) in agreement with the previously reported loss of CBs upon *abdA* overexpression [88].

Similarly, *btl*-Gal4 mediated overexpression of either *Ubx* or *abdA* restores the fusion defects of DT1 and DT2 in *ptc* mutants (S3N, O Fig.). We detected that expression of both *salm-TSE-lacZ* and *kni-(dpp)-lacZ* is restored in the dorsal part of Tr1 of *ptc* mutants upon *abdA* overexpression (S3P, Q Fig.). These results argue that the Hox code in the airway cells autonomously changes *hh*-signaling outputs in Tr1 both in wild type and in *ptc* mutants, where the *hh* pathway is hyper activated. Finally, we asked if transgenic expression of *abdA* or *Ubx* in the airways could restore the branch fusion defects along the entire DT of *Ubx abdA* double mutants. Again, this manipulation rescues the branch fusion phenotypes (S3R-T Fig.) arguing that BX-C genes autonomously shunt *hh* signaling from inducing *kni* in the DTa branches of all metameres to promote continuous DT formation.

BX-C genes control tube tapering

A common characteristic of biological tubes is the tapering of tube diameter along their length. The *Drosophila* larval airways receive air only from the PSP and distribute it anteriorly. Correspondingly, the tubes show a posterior to anterior tapering [38], which presumably gradually increases the flow rates to the anterior and facilitates air diffusion from the PSP to the most distant anterior organs (http://hyperphysics.phy-astr.gsu.edu/hbase/pfric.html).
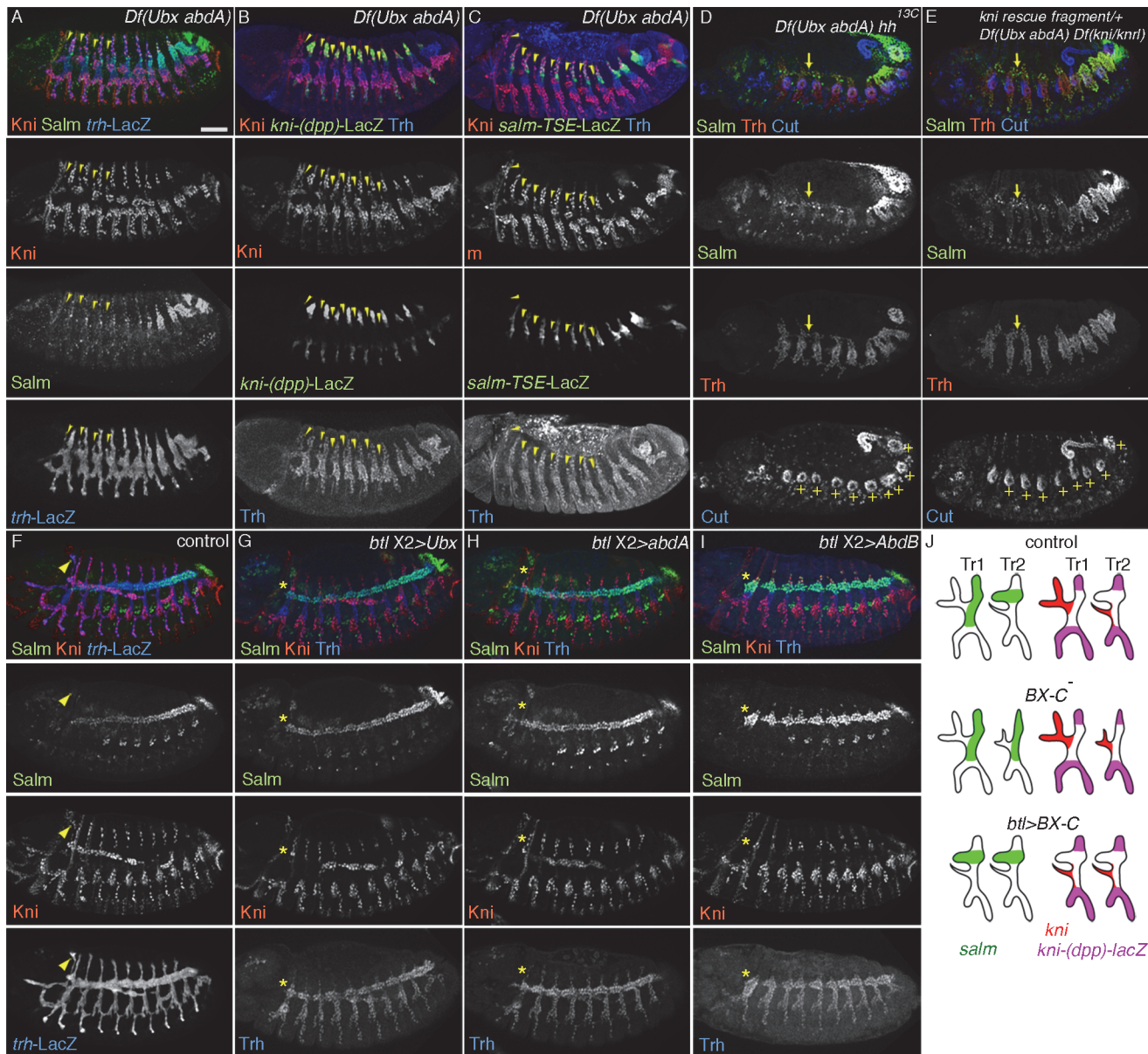
Figure 4. The airway intrinsic BX-C code determines the outcome of *hh* signaling. (A-C) Effects of loss of *Ubx* and *abdA* on the DTa fate in the central metameres. In *Df(Ubx abdA)* mutants at stage 13, ectopic dorsalword migration of cells that are positive for Kni and negative for Salm is variably detected in metameres 1–7 (A). These transformed DTa/CB-like cells (arrowheads) are negative for both *kni-(dpp)-lacZ* (B) and *salm-TSE-lacZ* (C). Note that expression of Salm/*salm-TSE*-LacZ is weakly detected in DB, DTp and TC in the transformed metameres as well as in Tr1. (D, E) Effects of *hh* or *kni/knrl* mutations on Salm expression in DTa of *Df(Ubx abdA)* mutants. Compared to *Df(Ubx abdA)* mutants (A-C), in *hh Df(Ubx abdA)* (D), or in *Df(kni/knrl) Df(Ubx abdA)* mutants, where early gap gene function of *kni* is rescued (E), Salm expression is equally detected in DTa and DTp. Note that the fusion of DT branches in the central metameres is weakly restored (arrows). This rescue is not due to an artificial collapse of the airway primordia because many of the ectopic Cut positive anterior spiracle (ASP) [125] (+, bottom panels) at the proximal part of the airway remain separate. (F-I) Effects of overexpression of BX-C genes on expression of Salm and Kni. In the control at stage 13 (F), CB (arrowhead) is positive for Kni and negative for Salm. Note that Salm expression in DT shows a posterior-to-anterior decrease. Upon overexpression of *Ubx* (G), *abdA* (H) or *AbdB* (I), DTa1 becomes negative for Kni and positive for Salm (asterisks). Note that the posterior-to-anterior decrease of Salm expression is variably disrupted, most prominently upon *AbdB* overexpression. Note that DB in all metameres strongly expresses Salm upon *AbdB* overexpression. (J) A summary of BX-C mutant conditions regarding primary branch identities. Scales bars: 50um.

doi:10.1371/journal.pgen.1004929.g004

salm is a master selector gene for DT identity. Intriguingly, its expression levels in the DT tubes at stage 13/14 show a largely proportional decrease from posterior to anterior metameres matching the tapering of the airways ([Fig. 4F](#))[30]. The graded diameter along the airway

length also coincides with the graded expression of BX-C proteins along the A-P axis. To explore the potential regulatory roles of BX-C factors and *salm* in tube shaping, we first analyzed airway shapes in BX-C mutants and detected 2 kinds of effects of BX-C genes on tube diameter, metamere-autonomous and systemic (see below).

Consistent with graded *AbdB* expression in PS 10–13, in *AbdB* mutants, tube diameter in DT7-10 lost its tapering and became narrower suggesting that the amount of *AbdB* proportionally controls the tube diameter. (Fig. 5A, C, I, J and S1 Table). Similarly, in *abdA* mutants, the gradient of tube diameter in DT4-6 was lost and DT4-9 became narrower (Fig. 5B, I, J and S1 Table) suggesting again that AbdA levels proportionally control DT tube diameter. In *abdA AbdB* double mutants the shape of the airways is changed further (Fig. 5D, I, J and S1 Table). The airways of Tr4-10 acquire a more cylindrical shape compared to the conically shaped tubes of wild type embryos. We suggest that in wild type embryos the gradient of *abdA* and *AbdB* activities would superimpose on a weak but clear, *abdA* and *AbdB*-independent gradient of DT tube thickness (Fig. 5I and S1 Table). This may explain why *abdA* mutants, where PS7-9 (DT4-6) are expected to transform to PS6 (DT3) still show a clear difference in tube diameter between DT3 and DT4 and why *AbdB* mutants, where PS10-13 (DT7-10) are expected to transform to PS9 (DT6) show a distinct tube caliber in DT6 and DT7 (Fig. 5I and S1 Table). Thus, in accord with their known functions in determining cell fates and morphogenesis in the embryonic ectoderm [39,44,53], the BX-C genes control the tapering of airways along the A-P axis autonomously. We note however that there is also a systemic effect of BX-C mutations along the entire DT. In either *abdA, AbdB* single or in *abdA AbdB* double mutants, the diameter of the more anterior metameres, where corresponding BX-C genes are not expressed also show a slight reduction of tube diameter (Fig. 5I and S1 Table). Among different possibilities, these results may suggest that the activities of *abdA* or *AbdB* control the hydrostatic pressure in the lumen to non-autonomously assure proportional growth of all the DT tubes [89] (see below). The residual tapering of *abdA AbdB* double mutants implies a mechanism of A-to-P gradient formation independent of *abdA* and *AbdB*. *Ubx* could exert such a function in the absence of *abdA* and *AbdB*. We analyzed bxd^{113} or bxd^{100} mutants, where Ubx expression levels in PS5 become similar to that of PS4 but its ectodermal expression is lost from PS7 onwards [90] (S4A Fig.). In these embryos, DT3 tube diameter approaches that of DT2 and there is also an overall reduction of tube diameter in more posterior metameres (Fig. 5I, S4C-E Fig. and S1 Table), suggesting that the endogenous Ubx level controls DT diametric tube expansion. However, in *abdA AbdB* double mutants, Ubx levels are largely uniform in DT4-10, which correspond to PS7-13 [91] (S5B Fig.). This suggests the presence of an additional, BX-C-independent cue in DT tube shaping. In *Ubx abdA AbdB* triple mutants, the transformed Salm positive residual DT/TC branches in posterior metameres are slightly thicker than those in anterior metameres, further arguing for the existence of the postulated BX-C-independent mechanism in tube shaping (S3K, S4F Figs.).

Is there any causative link between the BX-C mediated DT expansion control and the A-to-P gradual increase of *salm* expression levels in the DT (Fig. 4F) [30]? We noticed that Salm levels are reduced in central and posterior metameres of *abdA, AbdB* or *abdA AbdB* double mutants (S4G-J Fig.). This reduction is largely consistent with the changes in shape and DT tube diameters in the corresponding mutants. Conversely, upon overexpression of *AbdB*, higher Salm amounts are detected in the DT of all metameres at stage 13 (Fig. 4I). The DT branches of these embryos often stall and fail to fuse making evaluation of tube diameter difficult. Nevertheless, the DT diameter in all metameres appears comparable to the diameter of the most posterior DT branches (Fig. 5G). Overexpression of *Ubx* or *abdA* renders Salm expression levels uniform in the anterior metameres (Fig. 4G, H). Correspondingly, the DT diameter in the anterior metameres becomes thicker (Fig. 5E, F, I, J and S1 Table).
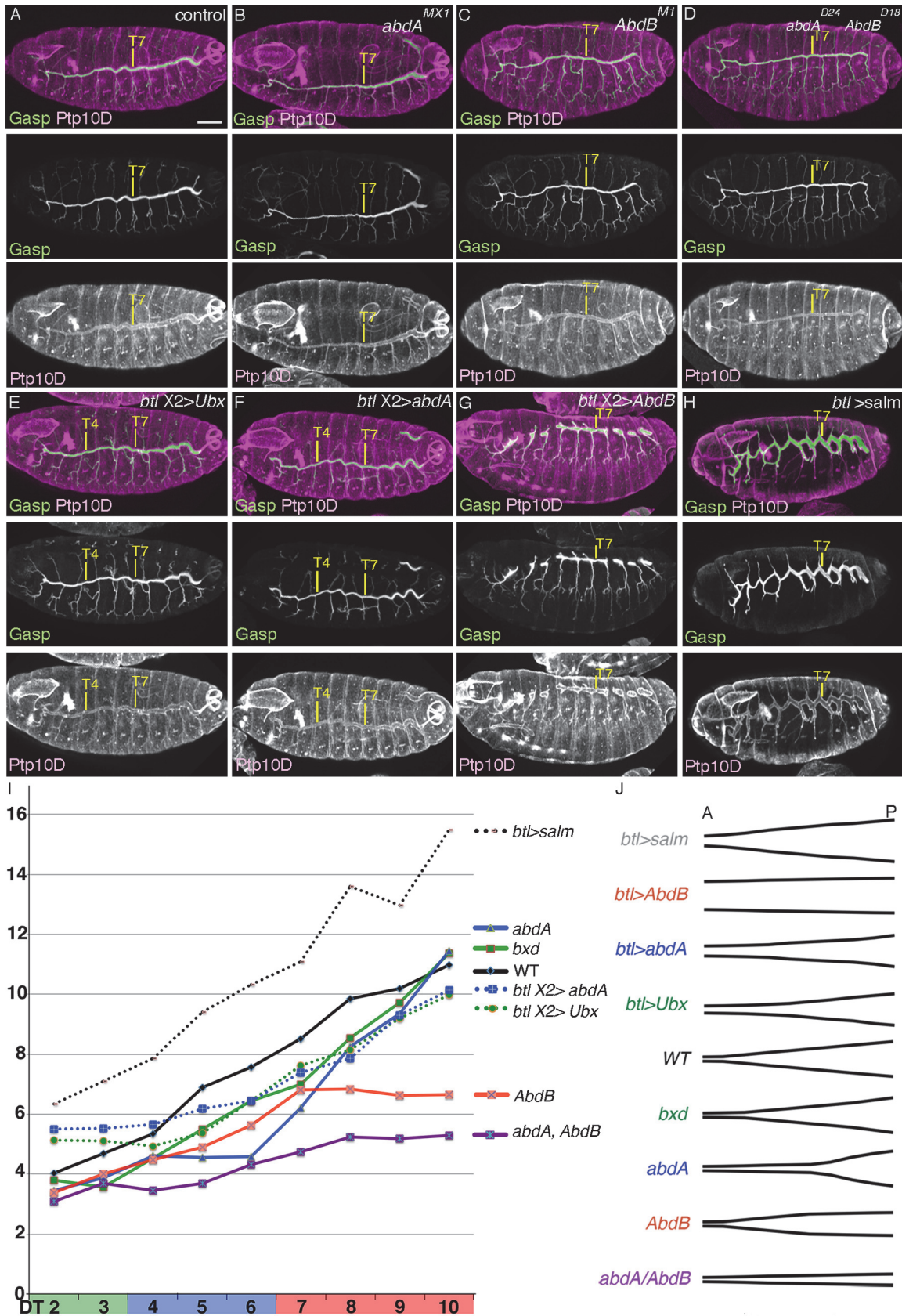
Figure 5. BX-C genes control DT tube tapering. (A-H) BX-C control of DT tube tapering visualized by luminal Gasp and the apical protein PTP10D. In the control (A), DT tube diameter shows posterior-to-anterior tapering. In *abdA* mutants, tube diameter of DT4-6 approaches that of DT3 while in *AbdB* mutants, tube diameter of DT7-10 resembles that of DT6. In *abdA AbdB* double mutants, tube diameter of DT4-10 resembles that of DT3. Note that there is still a weak tapering of the tube. Upon overexpression of *Ubx* (E) or *abdA* (F), tube diameter of DT2/3 becomes thicker than the control. We noticed that DT diameter in the posterior metameres becomes adversely reduced. This could be attributed to competition between the overexpressed proteins and endogenous *abdA* or *AbdB* [46], leading to a systemic decrease of tube diameter. Upon overexpression of *AbdB* (G), DT fusion becomes frequently defective. However, it is apparent that DT tube diameter of the anterior metameres resembles that of DT10. Upon overexpression of *salm* (H), DT tube diameter becomes thicker than the control. In addition, tube diameter of other branches also becomes thicker [28]. (I,J) Quantification (I) and cartoons (J) of diameter phenotypes of this figure and other figures are shown. Raw data used for quantification and some statistics are shown in S1 Table. See text for details. Scales bars: 50um.

How does the Salm gradient along the DT A-P axis correlate to the graded DT tube expansion? *salm* overexpression confers DT identity to other primary branches [28,62]. We noted that *salm* overexpression also generally expands tube diameter not only in the transformed branches [28] but also in the DT, which endogenously expresses *salm* (Fig. 5H, I, J and S1 Table). The programmed secretion of luminal and apical proteins has been proposed to drive tube dilation of the *Drosophila* airways [92–95]. Tenectin (Tnc) is a luminal glycoprotein accumulating in the DT and hindgut tubes during diametric expansion [96]. Tnc overexpression in the airways drives DT tube dilation in a dose-dependent manner potentially through increasing hydrostatic pressure [89] and the *tnc* mRNA levels increase in a characteristic graded fashion along the A-P axis of the DT tubes in wild type embryos [89]. We found that the diametric increase caused by *salm* overexpression in the airways is accompanied by an increase in the luminal levels of Tnc and conversely, Tnc becomes undetectable in the tracheal tubes of *salm* mutants (S4K-M Fig.). This suggests that Salm adjusts the graded expression levels of Tnc and presumably other proteins during tube dilation.

Additionally, the diameter increase in the branches of *salm* over expressing embryos is still most pronounced in the posterior metameres. (Fig. 5H, I, J and S1 Table). The accentuated tube enlargement in posterior metameres upon *salm* overexpression suggests a *salm*-independent control mode of A-to-P gradient of DT tube diameter. This is consistent with the observation that tube diameter of the remaining branches in *salm* mutants are still thickest in Tr10 (S4N Fig.).

In conclusion, our work suggests two interdependent mechanisms by which the tube intrinsic Hox code controls branch identity and tube shape in the *Drosophila* respiratory network (Fig. 6A, B). Firstly, Hox genes autonomously divert extrinsic *hh* signaling from *kni* induction in the DT thereby generating continuous, *salm* positive DT airways. We suggest that this allows a second tier of DT tube shape regulation, where the Hox activity gradient both locally and systemically organizes graded tube dilation via *salm* dependent and independent modes. The Ci/BX-C circuit may control tube morphology directly by binding to the regulatory regions of *kni* and *salm*, as recent genome-wide TF binding studies suggest that *kni* is a direct target of *ci* [37] and that *salm* is a direct target of *Ubx* [97]. In our model, tube tapering and thereby luminal fluid flow are calibrated by the balance between extrinsic signals and the intrinsic Hox code. Since Hox selector genes are regionally expressed in other developing tubular organs like the mammalian lung [98] and vasculature [9,10], a similar regulatory logic of tube branching and shaping may apply to other systems.

Materials and Methods

Fly genetics

Flies kept over balancer chromosomes [99] were grown in standard medium. We obtained the appropriate genotypes by standard genetic crosses. For overexpression of genes, we used the Gal4/UAS system [100]. Mutant embryos were identified by the expression of *twi-lacZ, ftz-*
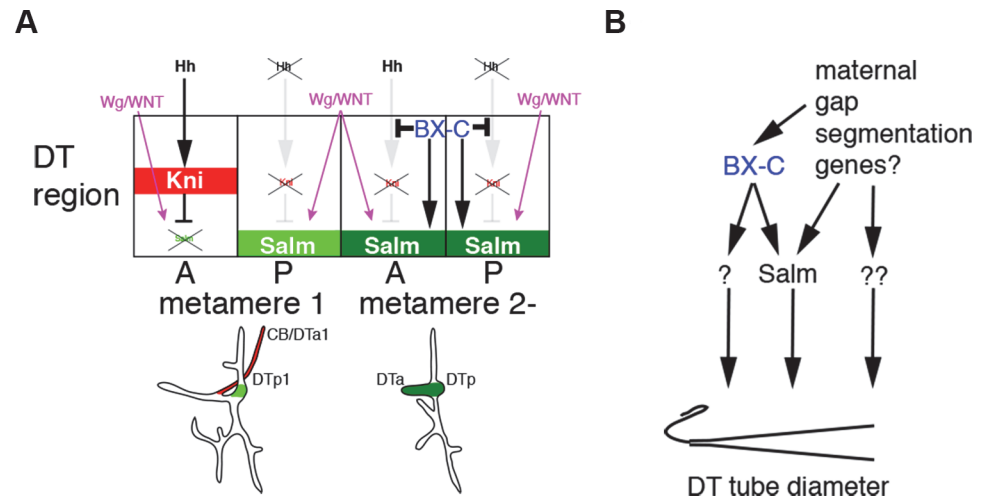
Figure 6. Models for the BX-C dependent control of branching patterns and of DT tube diameter. (A) In all metameres, expression of *hh* and *wg* in cells surrounding the tracheal primordia are comparable. In metamere 1, where there is no input from BX-C, *hh* signaling induces *kni* in DTa1 in wild type, and additionally in DTp1 in *ptc* mutants. *kni* represses *wg/WNT* mediated upregulation of *salm*, making DTa1 branches thinner. In the posterior metameres, BX-C shunts *hh* signaling from induction of *kni*, allowing *salm* upregulation by *wg/WNT*. BX-C additionally enhances *salm* expression in the DT. (B) BX-C genes coordinate the posterior-to-anterior tube tapering through *salm* dependent and independent modes. DT tube tapering may also be regulated independently of BX-C genes through inputs from the maternal, gap or segmentation gene cascades.

lacZ, Ubx-lacZ or dfd-GFP [101] constructs inserted on balancer chromosomes. We identified mutants harboring *Ubx* or *AbdB* mutations by selecting embryos with previously reported phenotypes in the anterior spiracle or PSP. For collection of large amount of virgins, we used a Y chromosome harboring *hs-hid* construct developed by R. Lehmann and M. Van Doren [102]. See Flybase [103] for details of strains described below.

Mutant strains. $abdA^{M1}$ (a gift from B. Gebelein) [104], $AbdB^{M1}$, $AbdB^{M5}$ and $Df(3R)P115$ as $Df(Ubx\ abdA\ AbdB)$ (gifts from I. Lohmann) [105], $btl^{\Delta oh10}$ and $btl^{\Delta oh24-1}$[106], $Df(5)$ as $Df(salm/salr)$ (a gift from M. Llimargas) [28,107], hh^{13C} [108], *kni early rescue fragment;* $Df(3L)riXT$ (a gift from R. Schuh) [25], rho^{d38} (a gift from D. Andrew and A. Salzberg) [109,110], rho^{7M} (a gift from J. Skeath) [111], top^{f24} (a gift from K. Moses) [112]. arm^4 and $CycA^3$ were obtained from Natinal Institute of Genetics (NIG), Mishima, Japan. Ubx^1, $abdA^{MX1}$, $abdA^{D24}\ AbdB^{D18}$, $Ubx^1\ abdA^{D24}\ AbdB^{D18}$[113], $Df(109)$ as $Df(Ubx,abdA)$, $CycA^{C8LR1,}$ $Df(3L)Exel6115$ as $Df(CycA)$, hh^{AC}, $Df(3L)BSC448$ homozygous or its transheterozygote over $Df(3L)riXT$ as $Df(kni/knrl)$, ptc^9, $Df(2R)Exel7098$ as $Df(ptc)$, smo^3, tkv^7 and $Df(2R)Exel6076$ as $Df(top)$ were obtained from Bloomington stock center (BDSC), Indiana, USA.

Enhancer trap strains. *1-eve-1* as *trh-lacZ* (a gift from N. Perrimon) [114] and $unpg^{r37}$ (a gift from F. J. Diaz-Benjumea, R. Urbach and G. M. Technau) [115,116]. hh^{P30} [117] was obtained from BDSC.

Enhancer reporter strains. *kni-(dpp)-lacZ* [25] and *salm-TSE-lacZ* [30] (gifts from R. Schuh).

Gal4 and UAS strains. *btl-gal4* on 2nd and 3rd chromosomes (gifts from S. Hayashi) [58], *UAS-abdA* (a gift from F. J. Diaz-Benjumea) [115], *UAS-ci^{75}* and *UAS-ci^{H4P}* (gifts from S. Ishii) [84], *UAS-ci^{rep}* (a gift from A. Moore) [83], *UAS-kni* and *UAS-knrl* (gifts from R. Schuh) [25]. *UAS-AbdB, UAS-Axn-GFP, UAS-salm* and *UAS-Ubx* were obtained from BDSC.

please format as a second level heading

Egg collection was done with apple/grape juice plate at 25°C. Embryos were bleached and fixed as previously described [118] for 15–30 minutes with a 1:1 mixture of heptane and a fix solution (3.7% formaldehyde, 0.1M Hepes pH6.9, 2mM MgSO4). Embryos were dechorionated with methanol and incubated in 0.1% PBT supplemented with 0.5% BSA. Staging of embryos was done as previously described [119].

For immunostaining the following primary antibodies were used:

Guinea-pig anti-AbdA (1:500, a gift from B. Gebelein) [104], rabbit anti-Dys (1:500, a gift from L. Jiang) [18], Guinea-pig anti-Gasp (1:1000) [95], mouse anti-Ubx (1:10, a gift from R. White) [120], Guinea-pig anti-Kni (1:300), (developed by J. Reinitz and distributed by Y. Hiromi, East Asian Segmentation Antibody Center, Mishima, Japan) [121], rabbit anti-Salm (1:200, gifts from R. Barrio and T. Cook) [107,122], rabbit anti-Tnc C-terminal (1:1000, a gift from Z. A. Syed and A. Uv) [89], rat anti-Trh (1:200, a gift from D. Andrew) [123] and rabbit anti-Trh (1:50). Mouse anti-Abd-B (1:10, donated by S. Celniker) [124], mouse anti-Cut (1:10, donated by G. M. Rubin) [125], mouse anti-Hnt (1:10, donated by H. D. Lipshitz) [126], mouse mab2A12 (anti-Gasp) (1:5, donated by M. Krasnow, N. Patel and C. Goodman) [17,95], mouse anti-Ptc (1:10, donated by I. Guerrero) [127] and mouse anti-PTP10D (1:10, donated by K. Zinn) [128] were obtained from Developmental Studies Hybridoma Bank (DSHB), Iowa, USA. Commercially available antibodies were anti-LacZ (*E.coli.* β-Galactosidase) antibodies made in goat (1:500, Biogenesis) or rabbit (1:1000, Capel) and anti-GFP antibodies made in rabbit (1:500, JL-8 Clontech), mouse (1:1000, GFP20 Sigma) or goat (1:500, ab6673 Abcam).

Donkey or goat biotin- or fluorescently labeled secondary antibodies made against the host species of primary antibodies were purchased from Jackson Laboratories. Streptavidin coupled with AMCA, FITC or Cy5 were used when necessary. For mab2A12 detection TSA amplification (PerkinElmer) was used.

Double fluorescent labeling with RNA probe and antibody was carried out as described [129]. The following cDNA clones were used to make hybridization probes; *bnl* (a gift from M. Krasnow) [20], *dpp* [108] and *unpg* (a gift from P. A. Beachy) [54]. *wg, salm* and *kni* clones were obtained from Drosophila Genomics Resource Center (DGRC), Indiana, USA.

Confocal images were taken by Biorad MRC1024, Oympus Fluoview 1000 or Zeiss LSM780. Images of controls and mutants taken by the same confocal microscopes were used for comparison. Images were processed by ImageJ and figures were prepared with Photoshop and Illustrator.

Quantification of Trh positive cell number of CB was done for stage 13 embryos stained with antibodies against Trh and DE-cad, scanned at 40× magnification with 0.6 um intervals.

For quantification of DT tube thickness, mid-late stage 16 embryos stained with antibodies against PTP10D, Gasp and DE-cad were scanned at 40× magnification with 0.6 um intervals. Using ImageJ, 3 points next to the bases of DB were selected from each Z-stacked image for each metamere to measure the maximal distance of PTP10D positive apical membranes perpendicular to the longitudinal tube axis. 3 embryos for each genotype were measured. Average, SD and p-value of student t-test were calculated by Excel.

Supporting Information

S1 Fig. Expression or potential functions of *dFGF/bnl, dEGFR, wg, dpp* and *hh* for DTa1/CB formation. DTa1 is marked with arrowhead or asterisks in the different panels.
(A-D) *bnl* signaling.
(A, B) Expression of *bnl*.
(A) At late stage 11, corresponding to the 6 primary branches of the airway (marked with *trh-lacZ*), 6 patches of surrounding cells express *bnl* for Tr1.

(B) At stage 12, DTa1 appears to extend toward *bnl* expression corresponding to the DB0 position.

(C, D) Expression of *kni* RNA.

Compared to the control (C), in *btl* mutants (D) at early stage 12, *kni* induction in DB is variably abolished while its DTa1 expression is comparable. Different magnification was used to image the same embryo in Fig. 1B and S1C Fig.

(E-F) *dEGFR* signaling.

In either *rho* mutant (E) or *dEGFR* mutant (F), Kni expression in DTa1/CB at stages 13–14 is comparable to the control (Fig. 1D).

(G-J) *wg* and *dpp* signaling.

wg RNA distribution (G) relative to DT or *dpp* RNA expression (H) in the dorsal and the lateral ectodermal stripes at stages11/12 are comparable in all metameres.

(I) In *arm* mutants at stage 13, expression of Kni as well *as kni-(dpp)*-LacZ in DB/LT/GB are comparable to the control (Fig. 1D).

(J) In *tkv* mutants at stage 13, *kni-(dpp)*-LacZ expression in DB/LT/GB is variably abolished while Kni expression in DTa1/CB is comparable to the control (Fig. 1D).

(K-O) *hh* signaling.

(K, L) Exterior (K) or interior (L) sections of Hh expression monitored with a *hh* enhancer trap line. *hh* is detected just above the anterior part of the invaginated airway primodia for all metameres (marked with Trh).

(M) In *hh* mutants at stage 12, *bnl* expression corresponding to DB extension is significantly decreased (cross). The ectodermal patches of *bnl* expression corresponding to DT extension become continuous.

(N, O) Gasp positive airway branching in *hh* or *smo* mutants.

(N) *hh* mutants have variable defects including loss or stalling of branches (DB, DT, VB or CB) or loss of metameres. CB does not form dorsal extension. (O) *smo* mutants often show CB misrouting phenotypes.

Scales bars: 50um.

(TIF)

S2 Fig. Effects of *hh* signaling overactivation on airway branching. (A-D) Effects of *ptc* or *CycA* mutations on expression of *kni* or *salm*. A summary of *ptc* mutant phenotypes is shown in (C).

(A, B) In *ptc/Df(ptc)* mutants, expression of *salm-TSE-lacZ* (A) and *kni-(dpp)-lacZ* (B) is lost in the dorsal part of the metamere 1 (asterisks) while Kni protein is expressed in the whole distal trachea in Tr1 (B, bottom panel).

(D) In *CycA* mutants, where the cell number in the airways is reduced nearly to half [38], DBs in all metameres express *kni-(dpp)-lacZ* comparably (arrows) and CB formation can occur (arrowheads).

(E-J) Stage 14–15 embryos stained with Gasp and Dys.

In the control (E), the fusion point of DT1/2 is occupied by two fusion cells originating from DTp1 and DTa2 (arrow).

In *ptc* mutants (F, G), *dys* expression is not detected in the positions of DT1p (and LT1p) (asterisks) while *CycA* mutant embryos (H) are comparable to the control (arrow).

btl-Gal4 driven Ci^{rep} (I) restores Dys positive fusion cells in DTp1 as well as fusion of DT1/2 (arrow).

Overexpression of Ci^{act} with *btl*-Gal4 (J) can mimic the phenotypes of *ptc* mutants. Dys expression in DTp1 position is lost and is accompanied by fusion defects of DT1/2 (asterisk).

Scales bars: 50um.
(TIF)

S3 Fig. Expression and functions of BX-C Hox genes in relation to airway development.
(A-D) Expression of BX-C genes at stage 13 visualized by the respective antibodies. A summary of the expression patterns is shown in (D).

(A) *Ubx* expression starts from metamere 2 and peaks at metamere 3. From metamere 3 to 10, *Ubx* expression forms a gradient.

(B) *abdA* expression starts from metamere 4 and peaks at metamere 6. From metamere 7 to 10, *abdA* expression forms a gradient.

Only the anterior half of metamere 10 expresses *Ubx* and *abdA*.

(C) *AbdB* expression starts in metamere 7 and peaks at metamere 10, forming a single gradient.

(E-K) Airway branching phenotypes of BX-C mutants assessed at stage 15 with expression of Gasp, Dys and Cut.

In the control (E), DT is continuous with a pair of Dys positive fusion cells at each fusion point (arrowhead for DT1/2). The terminal parts of the airway are plugged with Cut positive ASP and PSP (arrows) [125].

In *Ubx* mutants (E), metameres 2/3 are transformed to metamere 1 as judged by the loss of fusion cells at the position of DTa (asterisks) and gain of Cut positive ASP (marked with +). While *abdA* mutants (F) are largely normal, both *AbdB* single mutants (H) and *abdA AbdB* double mutants (I) have an ectopic fusion cell in DTp10 (asterisks), in addition to loss of Cut positive PSP (crosses).

In *Df(Ubx abdA)* mutants (J), in addition to metameres 2/3, metameres 4–6 are transformed to Tr1 while transformation is variable in Tr7-9. Namely, Dys-positive fusion cells at the position of DTa are lost in Tr2-8 while Tr 9 has 1–2 fusion cell. Fusion of DT9/10 is frequently observed. Cut positive ectopic ASPs are detected in Tr2-9 (marked by +). DTp diameter in Tr7-10 looks thicker compared to the more anterior metameres.

In *Ubx abdA AbdB* triple mutants (K), all metameres are transformed to Tr1. Cut-positive PSP is lost (cross). Instead, Cut positive ASP (+) as well as loss of fusion cell fates at the position of DTa (asterisks) is observed in all metameres. Note that in *Ubx, Df(Ubx abdA)* and *Ubx abdA AbdB* mutants, CB-like branches are variably detected in the transformed metameres [54].

(L, M) Effects of *hh* or *kni/knrl* mutations on DT of *Df(Ubx abdA)* mutants.

In *hh Df(Ubx abd)* mutants (L) or in *Df(kni/knrl) Df(Ubx abdA)* mutants, DT fusion is partially restored (arrows). Note that this rescue is not due to a fusion of the airway primordia because many of the ectopic Cut positive ASPs at the proximal part of the airway are separate.

(N-Q) Effects of overexpression of *Ubx* or *abdA* on *ptc* mutant phenolypes in Tr1.

Compared to *ptc* mutants (S2 Fig.), ectopically supplied *Ubx* (N) or *abdA* (O) in the airway cells significantly restores both fusion cell fates in DTa1 and subsequent fusion of DT1/2 (arrowheads). Similarly, *abdA* overexpression in *ptc* mutants restores expression of *kni-(dpp)-lacZ* (P) and *salm-TSE-lacZ* (Q) to metamere 1.

(R-T) Effects of overexpression of *Ubx* or *abdA* to the airway branching of *Ubx abdA* double mutants.

In *Df(Ubx abdA)/Df(Ubx abdA AbdB)* transheterozygote (R), Cut positive ASPs are detected in metameres 1–9. And frequent DT fusion occurs only in DT9/10. The airway specific overexpression of *Ubx* (S) or *abdA* (T) partially restores DT fusion (arrows). Note that *bnl* expression guiding DT branches are intact in the absence of BX-C complex [130].

Scales bars: 50um.
(TIF)

S4 Fig. *salm* dependent and independent airway tube tapering by BX-C and a potential *salm* target for tube tapering. (A-C, F) DT tube tapering visualized by Gasp and PTP10D. Compared to the control (A) where DT3 is slightly thicker than DT2, in *bxd*[100] (B) or *bxd*[113] (C) mutants, DT3 becomes comparable or slightly narrower than DT2. In BX-C triple mutants (F), the posterior metameres tend to show slightly thicker DT tubes (arrows).

(D, E) Ubx expression in BX-C mutants a stage 13/14.

In *bxd*[113] mutants (D), Ubx expression in DT3 becomes comparable to the level in DT2 while in *abdA AbdB* double mutants, Ubx expression in DT4-10 becomes comparable to the level in DT3.

(G-J) Effects of *abdA* and/or *AbdB* mutations on Salm expression in DT.

In the control (G), Salm expression level forms a posterior-to-anterior gradient. In *abdA* mutants (H), Salm expression in the central metameres becomes comparable to the more anterior metameres while in *AbdB* mutants (I) Salm expression in the posterior metameres becomes comparable to the central metameres. In *abdA AbdB* double mutants (J), the Salm gradient becomes more flat, but a weak gradient is still detected.

(K-M) Effects of *salm* on Tnc expression in DT.

In the control (K) at stage 16, Tnc is secreted into the lumen but is locally detected in DT and TC1, both of which express *salm*. Expression of both Tnc and Salm appears slightly stronger in fusion points. Note that Tnc is also expressed in hindgut and the proximal part of PSP. Upon overexpression of *salm* (L) Tnc is detected in lumens of additional branches like TC (arrow). In Df(*salm/salr*) mutants where both *salm* and the neighboring *spalt-related* (*salr*) are deleted, Tnc expression in the airway is lost (M, asterisk), although its expression in PSP and hindgut remains.

(N) In Df(*salm/salr)* mutants, TC branches in the posterior metameres are thicker than in the anterior.

Scales bars: 50um.

(TIF)

S1 Table. DT thickness of various tube diameter mutants. Genotypes are; Wild type = Canton S, *bxd* = *bxd*[113], *abdA* = *abdA*[MX], *AbdB* = *AbdB*[M1] / *AbdB*[M5], *abdA AbdB* = *abdA*[D24] *AbdB*[D18].
Table A. Raw data of DT thickness in micrometers. For each genotype, 3 embryos were measured for DT thickness. 3 points of each DT near the base of DB were measured.
Table B. Statistics of the raw data. Average thickness, standard deviation (SD) and p-value of student t-test are shown for each DT. For p-value, comparison between WT and each mutant is shown. For wt, bxd, abdA, AbdB single or abdA AbdB double mutants, additional comparison is shown between different metameres or between mutants. p<0.05 is judged to be significant.
(XLSX)

Acknowledgments

Author Contributions

Conceived and designed the experiments: RM. Performed the experiments: RM CH. Analyzed the data: RM. Contributed reagents/materials/analysis tools: KS CS. Wrote the paper: RM CS. Supported RM to drive the project: CS. Collected data for quantification: CH. Collected data for the other experiments: RM. Drafted the manuscript: RM. Contributed to finalize writing: CH KS.

References

1. Lubarsky B, Krasnow MA (2003) Tube morphogenesis: making and shaping biological tubes. Cell 112: 19–28. PMID: 12526790

2. Andrew DJ, Ewald AJ (2010) Morphogenesis of epithelial tubes: Insights into tube formation, elongation, and elaboration. Dev Biol 341: 34–55. doi: 10.1016/j.ydbio.2009.09.024 PMID: 19778532

3. Ochoa-Espinosa A, Affolter M (2012) Branching morphogenesis: from cells to organs and back. Cold Spring Harb Perspect Biol 4.

4. Kusumbe AP, Ramasamy SK, Adams RH (2014) Coupling of angiogenesis and osteogenesis by a specific vessel subtype in bone. Nature 507: 323–328. doi: 10.1038/nature13145 PMID: 24646994

5. Eilken HM, Adams RH (2010) Dynamics of endothelial cell behavior in sprouting angiogenesis. Curr Opin Cell Biol 22: 617–625. doi: 10.1016/j.ceb.2010.08.010 PMID: 20817428

6. Ghabrial A, Luschnig S, Metzstein MM, Krasnow MA (2003) Branching morphogenesis of the Drosophila tracheal system. Annu Rev Cell Dev Biol 19: 623–647. PMID: 14570584

7. Cantile M, Schiavo G, Terracciano L, Cillo C (2008) Homeobox genes in normal and abnormal vasculogenesis. Nutr Metab Cardiovasc Dis 18: 651–658. doi: 10.1016/j.numecd.2008.08.001 PMID: 19013779

8. Kachgal S, Mace KA, Boudreau NJ (2012) The dual roles of homeobox genes in vascularization and wound healing. Cell Adh Migr 6: 457–470. doi: 10.4161/cam.22164 PMID: 23076135

9. Pruett ND, Hajdu Z, Zhang J, Visconti RP, Kern MJ, et al. (2012) Changing topographic Hox expression in blood vessels results in regionally distinct vessel wall remodeling. Biol Open 1: 430–435. doi: 10.1242/bio.2012039 PMID: 23213434

10. Pruett ND, Visconti RP, Jacobs DF, Scholz D, McQuinn T, et al. (2008) Evidence for Hox-specified positional identities in adult vasculature. BMC Dev Biol 8: 93. doi: 10.1186/1471-213X-8-93 PMID: 18826643

11. Schottenfeld J, Song Y, Ghabrial AS (2010) Tube continued: morphogenesis of the Drosophila tracheal system. Curr Opin Cell Biol 22: 633–639. doi: 10.1016/j.ceb.2010.07.016 PMID: 20739171

12. Affolter M, Caussinus E (2008) Tracheal branching morphogenesis in Drosophila: new insights into cell behaviour and organ architecture. Development 135: 2055–2064. doi: 10.1242/dev.014498 PMID: 18480161

13. Manning G, Krasnow MA (1993) The Development of Drosophila melanogaster. Plainview, N.Y.: Cold Spring Harbor Laboratory Press.

14. Samakovlis C, Hacohen N, Manning G, Sutherland DC, Guillemin K, et al. (1996) Development of the Drosophila tracheal system occurs by a series of morphologically distinct but genetically coupled branching events. Development 122: 1395–1407. PMID: 8625828

15. Hartenstein V, Jan YN (1992) Studying Drosophila Embryogenesis with P-Lacz Enhancer Trap Lines. Rouxs Archives of Developmental Biology 201: 194–220.

16. Tanaka-Matakatsu M, Uemura T, Oda H, Takeichi M, Hayashi S (1996) Cadherin-mediated cell adhesion and cell motility in Drosophila trachea regulated by the transcription factor Escargot. Development 122: 3697–3705. PMID: 9012491

17. Samakovlis C, Manning G, Steneberg P, Hacohen N, Cantera R, et al. (1996) Genetic control of epithelial tube fusion during Drosophila tracheal development. Development 122: 3531–3536. PMID: 8951068

18. Jiang L, Crews ST (2003) The Drosophila dysfusion basic helix-loop-helix (bHLH)-PAS gene controls tracheal fusion and levels of the tracheless bHLH-PAS protein. Mol Cell Biol 23: 5625–5637. doi: 10.1128/MCB.23.16.5625-5637.2003 PMID: 12897136

19. Uv A, Cantera R, Samakovlis C (2003) Drosophila tracheal morphogenesis: intricate cellular solutions to basic plumbing problems. Trends Cell Biol 13: 301–309. PMID: 12791296

20. Sutherland D, Samakovlis C, Krasnow MA (1996) branchless encodes a Drosophila FGF homolog that controls tracheal cell migration and the pattern of branching. Cell 87: 1091–1101. PMID: 8978613

21. Klambt C, Glazer L, Shilo BZ (1992) breathless, a Drosophila FGF receptor homolog, is essential for migration of tracheal and specific midline glial cells. Genes Dev 6: 1668–1678. PMID: 1325393

22. Reichman-Fried M, Dickson B, Hafen E, Shilo BZ (1994) Elucidation of the role of breathless, a Drosophila FGF receptor homolog, in tracheal cell migration. Genes Dev 8: 428–439. PMID: 8125257

23. Lee T, Hacohen N, Krasnow M, Montell DJ (1996) Regulated Breathless receptor tyrosine kinase activity required to pattern cell migration and branching in the Drosophila tracheal system. Genes Dev 10: 2912–2921. PMID: 8918892

24. Vincent S, Ruberte E, Grieder NC, Chen CK, Haerry T, et al. (1997) DPP controls tracheal cell migration along the dorsoventral body axis of the Drosophila embryo. Development 124: 2741–2750. PMID: 9226445

25. Chen CK, Kuhnlein RP, Eulenberg KG, Vincent S, Affolter M, et al. (1998) The transcription factors KNIRPS and KNIRPS RELATED control cell migration and branch morphogenesis during Drosophila tracheal development. Development 125: 4959–4968. PMID: 9811580

26. Ribeiro C, Ebner A, Affolter M (2002) In vivo imaging reveals different cellular functions for FGF and Dpp signaling in tracheal branching morphogenesis. Dev Cell 2: 677–683. PMID: 12015974

27. Chihara T, Hayashi S (2000) Control of tracheal tubulogenesis by Wingless signaling. Development 127: 4433–4442. PMID: 11003842

28. Llimargas M (2000) Wingless and its signalling pathway have common and separable functions during tracheal development. Development 127: 4407–4417. PMID: 11003840

29. Llimargas M, Lawrence PA (2001) Seven Wnt homologues in Drosophila: a case study of the developing tracheae. Proc Natl Acad Sci U S A 98: 14487–14492. doi: 10.1073/pnas.251304398 PMID: 11717401

30. Kuhnlein RP, Schuh R (1996) Dual function of the region-specific homeotic gene spalt during Drosophila tracheal system development. Development 122: 2215–2223. PMID: 8681802

31. Ribeiro C, Neumann M, Affolter M (2004) Genetic control of cell intercalation during tracheal morphogenesis in Drosophila. Curr Biol 14: 2197–2207. PMID: 15620646

32. Shaye DD, Casanova J, Llimargas M (2008) Modulation of intracellular trafficking regulates cell intercalation in the Drosophila trachea. Nat Cell Biol 10: 964–970. doi: 10.1038/ncb1756 PMID: 18641639

33. Buti E, Mesquita D, Araujo SJ (2014) Hedgehog is a positive regulator of FGF signalling during embryonic tracheal cell migration. PLoS One 9: e92682. doi: 10.1371/journal.pone.0092682 PMID: 24651658

34. Glazer L, Shilo BZ (2001) Hedgehog signaling patterns the tracheal branches. Development 128: 1599–1606. PMID: 11290298

35. Kato K, Chihara T, Hayashi S (2004) Hedgehog and Decapentaplegic instruct polarized growth of cell extensions in the Drosophila trachea. Development 131: 5253–5261. PMID: 15456724

36. Llimargas M, Casanova J (1997) ventral veinless, a POU domain transcription factor, regulates different transduction pathways required for tracheal branching in Drosophila. Development 124: 3273–3281. PMID: 9310322

37. Biehs B, Kechris K, Liu S, Kornberg TB (2010) Hedgehog targets in the Drosophila embryo and the mechanisms that generate tissue-specific outputs of Hedgehog signaling. Development 137: 3887–3898. doi: 10.1242/dev.055871 PMID: 20978080

38. Beitel GJ, Krasnow MA (2000) Genetic control of epithelial tube size in the Drosophila tracheal system. Development 127: 3271–3282. PMID: 10887083

39. Lewis EB (1978) A gene complex controlling segmentation in Drosophila. Nature 276: 565–570. PMID: 103000

40. Carroll SB (1995) Homeotic genes and the evolution of arthropods and chordates. Nature 376: 479–485. PMID: 7637779

41. Mann RS, Morata G (2000) The developmental and molecular biology of genes that subdivide the body of Drosophila. Annu Rev Cell Dev Biol 16: 243–271. PMID: 11031237

42. Shubin N, Tabin C, Carroll S (2009) Deep homology and the origins of evolutionary novelty. Nature 457: 818–823. doi: 10.1038/nature07891 PMID: 19212399

43. Mann RS, Carroll SB (2002) Molecular mechanisms of selector gene function and evolution. Curr Opin Genet Dev 12: 592–600. PMID: 12200165

44. Pearson JC, Lemons D, McGinnis W (2005) Modulating Hox gene functions during animal body patterning. Nat Rev Genet 6: 893–904. PMID: 16341070

45. Mallo M, Wellik DM, Deschamps J (2010) Hox genes and regional patterning of the vertebrate body plan. Dev Biol 344: 7–15. doi: 10.1016/j.ydbio.2010.04.024 PMID: 20435029

46. Castelli-Gair J, Greig S, Micklem G, Akam M (1994) Dissecting the temporal requirements for homeotic gene function. Development 120: 1983–1995. PMID: 7925003

47. Averof M, Akam M (1995) Hox genes and the diversification of insect and crustacean body plans. Nature 376: 420–423. PMID: 7630416

48. Averof M, Patel NH (1997) Crustacean appendage evolution associated with changes in Hox gene expression. Nature 388: 682–686. PMID: 9262403

49. Merabet S, Hombria JC, Hu N, Pradel J, Graba Y (2005) Hox-controlled reorganisation of intrasegmental patterning cues underlies Drosophila posterior spiracle organogenesis. Development 132: 3093–3102. PMID: 15930099

50. Sanchez-Higueras C, Sotillos S, Castelli-Gair Hombria J (2014) Common origin of insect trachea and endocrine organs from a segmentally repeated precursor. Curr Biol 24: 76–81. doi: 10.1016/j.cub.2013.11.010 PMID: 24332544

51. Kaufman TC, Lewis R, Wakimoto B (1980) Cytogenetic Analysis of Chromosome 3 in DROSOPHILA MELANOGASTER: The Homoeotic Gene Complex in Polytene Chromosome Interval 84a-B. Genetics 94: 115–133. PMID: 17248988

52. Sanchez-Herrero E, Vernos I, Marco R, Morata G (1985) Genetic organization of Drosophila bithorax complex. Nature 313: 108–113. PMID: 3917555

53. Maeda RK, Karch F (2006) The ABC of the BX-C: the bithorax complex explained. Development 133: 1413–1422. PMID: 16556913

54. Chiang C, Young KE, Beachy PA (1995) Control of Drosophila tracheal branching by the novel homeodomain gene unplugged, a regulatory target for genes of the bithorax complex. Development 121: 3901–3912. PMID: 8582298

55. Hu N, Castelli-Gair J (1999) Study of the posterior spiracles of Drosophila as a model to understand the genetic and cellular mechanisms controlling morphogenesis. Dev Biol 214: 197–210. PMID: 10491268

56. Nusslein-Volhard C, Wieschaus E (1980) Mutations affecting segment number and polarity in Drosophila. Nature 287: 795–801. PMID: 6776413

57. Chung S, Chavez C, Andrew DJ (2011) Trachealess (Trh) regulates all tracheal genes during Drosophila embryogenesis. Dev Biol 360: 160–172. doi: 10.1016/j.ydbio.2011.09.014 PMID: 21963537

58. Shiga Y, TanakaMatakatsu M, Hayashi S (1996) A nuclear GFP beta-galactosidase fusion protein as a marker for morphogenesis in living Drosophila. Development Growth & Differentiation 38: 99–106.

59. Hamada F, Tomoyasu Y, Takatsu Y, Nakamura M, Nagai S, et al. (1999) Negative regulation of Wingless signaling by D-axin, a Drosophila homolog of axin. Science 283: 1739–1742. PMID: 10073940

60. Willert K, Logan CY, Arora A, Fish M, Nusse R (1999) A Drosophila Axin homolog, Daxin, inhibits Wnt signaling. Development 126: 4165–4173. PMID: 10457025

61. Cliffe A, Hamada F, Bienz M (2003) A role of Dishevelled in relocating Axin to the plasma membrane during wingless signaling. Curr Biol 13: 960–966. PMID: 12781135

62. Caviglia S, Luschnig S (2013) The ETS domain transcriptional repressor Anterior open inhibits MAP kinase and Wingless signaling to couple tracheal cell fate with branch identity. Development 140: 1240–1249. doi: 10.1242/dev.087874 PMID: 23444354

63. Price JV, Clifford RJ, Schupbach T (1989) The maternal ventralizing locus torpedo is allelic to faint little ball, an embryonic lethal, and encodes the Drosophila EGF receptor homolog. Cell 56: 1085–1092. PMID: 2493993

64. Wappner P, Gabay L, Shilo BZ (1997) Interactions between the EGF receptor and DPP pathways establish distinct cell fates in the tracheal placodes. Development 124: 4707–4716. PMID: 9409686

65. Rutledge BJ, Zhang K, Bier E, Jan YN, Perrimon N (1992) The Drosophila spitz gene encodes a putative EGF-like growth factor involved in dorsal-ventral axis formation and neurogenesis. Genes Dev 6: 1503–1517. PMID: 1644292

66. Bier E, Jan LY, Jan YN (1990) rhomboid, a gene required for dorsoventral axis establishment and peripheral nervous system development in Drosophila melanogaster. Genes Dev 4: 190–203. PMID: 2110920

67. Urban S, Lee JR, Freeman M (2001) Drosophila rhomboid-1 defines a family of putative intramembrane serine proteases. Cell 107: 173–182. PMID: 11672525

68. Affolter M, Nellen D, Nussbaumer U, Basler K (1994) Multiple requirements for the receptor serine/threonine kinase thick veins reveal novel functions of TGF beta homologs during Drosophila embryogenesis. Development 120: 3105–3117. PMID: 7720555

69. Nellen D, Affolter M, Basler K (1994) Receptor serine/threonine kinases implicated in the control of Drosophila body pattern by decapentaplegic. Cell 78: 225–237. PMID: 8044837

70. Wieschaus E, Nussleinvolhard C, Jurgens G (1984) Mutations Affecting the Pattern of the Larval Cuticle in Drosophila-Melanogaster .3. Zygotic Loci on the X-Chromosome and 4th Chromosome. Wilhelm Rouxs Archives of Developmental Biology 193: 296–307.

71. Noordermeer J, Klingensmith J, Perrimon N, Nusse R (1994) dishevelled and armadillo act in the wingless signalling pathway in Drosophila. Nature 367: 80–83. PMID: 7906389

72. Siegfried E, Wilder EL, Perrimon N (1994) Components of wingless signalling in Drosophila. Nature 367: 76–80. PMID: 8107779

73. Jiang J, Hui CC (2008) Hedgehog signaling in development and cancer. Dev Cell 15: 801–812. doi: 10.1016/j.devcel.2008.11.010 PMID: 19081070

74. Chen Y, Jiang J (2013) Decoding the phosphorylation code in Hedgehog signal transduction. Cell Res 23: 186–200. doi: 10.1038/cr.2013.10 PMID: 23337587

75. Hidalgo A, Ingham P (1990) Cell patterning in the Drosophila segment: spatial regulation of the segment polarity gene patched. Development 110: 291–301. PMID: 2081466

76. Ingham PW (1993) Localized hedgehog activity controls spatial limits of wingless transcription in the Drosophila embryo. Nature 366: 560–562. PMID: 8255293

77. DiNardo S, Heemskerk J, Dougan S, O'Farrell PH (1994) The making of a maggot: patterning the Drosophila embryonic epidermis. Curr Opin Genet Dev 4: 529–534. PMID: 7950320

78. Aza-Blanc P, Ramirez-Weber FA, Laget MP, Schwartz C, Kornberg TB (1997) Proteolysis that is inhibited by hedgehog targets Cubitus interruptus protein to the nucleus and converts it to a repressor. Cell 89: 1043–1053. PMID: 9215627

79. Methot N, Basler K (1999) Hedgehog controls limb development by regulating the activities of distinct transcriptional activator and repressor forms of Cubitus interruptus. Cell 96: 819–831. PMID: 10102270

80. Methot N, Basler K (2001) An absolute requirement for Cubitus interruptus in Hedgehog signaling. Development 128: 733–742. PMID: 11171398

81. Parker DS, White MA, Ramos AI, Cohen BA, Barolo S (2011) The cis-regulatory logic of Hedgehog gradient responses: key roles for gli binding affinity, competition, and cooperativity. Sci Signal 4: ra38. doi: 10.1126/scisignal.2002077 PMID: 21653228

82. Hepker J, Wang QT, Motzny CK, Holmgren R, Orenic TV (1997) Drosophila cubitus interruptus forms a negative feedback loop with patched and regulates expression of Hedgehog target genes. Development 124: 549–558. PMID: 9053330

83. Karim MR, Moore AW (2011) Convergent local identity and topographic projection of sensory neurons. J Neurosci 31: 17017–17027. doi: 10.1523/JNEUROSCI.2815-11.2011 PMID: 22114271

84. Dai P, Akimaru H, Ishii S (2003) A hedgehog-responsive region in the Drosophila wing disc is defined by debra-mediated ubiquitination and lysosomal degradation of Ci. Dev Cell 4: 917–928. PMID: 12791275

85. Martizez Arias A, Baker NE, Ingham PW (1988) Role of segment polarity genes in the definition and maintenance of cell states in the Drosophila embryo. Development 103: 157–170. PMID: 3197626

86. Wilk R, Weizman I, Shilo BZ (1996) tracheless encodes a bHLH-PAS protein that is an inducer of tracheal cell fates in Drosophila. Genes Dev 10: 93–102. PMID: 8557198

87. Chen Y, Gallaher N, Goodman RH, Smolik SM (1998) Protein kinase A directly regulates the activity and proteolysis of cubitus interruptus. Proc Natl Acad Sci U S A 95: 2349–2354. PMID: 9482888

88. Merabet S, Litim-Mecheri I, Karlsson D, Dixit R, Saadaoui M, et al. (2011) Insights into Hox protein function from a large scale combinatorial analysis of protein domains. PLoS Genet 7: e1002302. doi: 10.1371/journal.pgen.1002302 PMID: 22046139

89. Syed ZA, Bouge AL, Byri S, Chavoshi TM, Tang E, et al. (2012) A luminal glycoprotein drives dose-dependent diameter expansion of the Drosophila melanogaster hindgut tube. PLoS Genet 8: e1002850. doi: 10.1371/journal.pgen.1002850 PMID: 22876194

90. Camprodon FJ, Castelligair JE (1994) Ultrabithorax Protein Expression in Breakpoint Mutants—Localization of Single, Cooperative and Redundant Cis Regulatory Elements. Rouxs Archives of Developmental Biology 203: 411–421.

91. Struhl G, White RA (1985) Regulation of the Ultrabithorax gene of Drosophila by other bithorax complex genes. Cell 43: 507–519. PMID: 3935322

92.   Tsarouhas V, Senti KA, Jayaram SA, Tiklova K, Hemphala J, et al. (2007) Sequential pulses of apical epithelial secretion and endocytosis drive airway maturation in Drosophila. Dev Cell 13: 214–225. PMID: 17681133

93.   Forster D, Luschnig S (2012) Src42A-dependent polarized cell shape changes mediate epithelial tube elongation in Drosophila. Nat Cell Biol 14: 526–534. doi: 10.1038/ncb2456 PMID: 22446736

94.   Forster D, Armbruster K, Luschnig S (2010) Sec24-dependent secretion drives cell-autonomous expansion of tracheal tubes in Drosophila. Curr Biol 20: 62–68. doi: 10.1016/j.cub.2009.11.062 PMID: 20045324

95.   Tiklova K, Tsarouhas V, Samakovlis C (2013) Control of airway tube diameter and integrity by secreted chitin-binding proteins in Drosophila. PLoS One 8: e67415. doi: 10.1371/journal.pone.0067415 PMID: 23826295

96.   Fraichard S, Bouge AL, Chauvel I, Bouhin H (2006) Tenectin, a novel extracellular matrix protein expressed during Drosophila melanogaster embryonic development. Gene Expr Patterns 6: 772–776. PMID: 16510317

97.   Choo SW, White R, Russell S (2011) Genome-wide analysis of the binding of the Hox protein Ultrabithorax and the Hox cofactor Homothorax in Drosophila. PLoS One 6: e14778. doi: 10.1371/journal.pone.0014778 PMID: 21483667

98.   Herriges JC, Yi L, Hines EA, Harvey JF, Xu G, et al. (2012) Genome-scale study of transcription factor expression in the branching mouse lung. Dev Dyn 241: 1432–1453. doi: 10.1002/dvdy.23823 PMID: 22711520

99.   Lindsley DL, Zimm GG, Lindsley DL (1992) The genome of Drosophila melanogaster. San Diego: Academic Press. viii, 1133 p., 1138 leaves of plates p.

100. Brand AH, Perrimon N (1993) Targeted gene expression as a means of altering cell fates and generating dominant phenotypes. Development 118: 401–415. PMID: 8223268

101. Le T, Liang Z, Patel H, Yu MH, Sivasubramaniam G, et al. (2006) A new family of Drosophila balancer chromosomes with a w-dfd-GMR yellow fluorescent protein marker. Genetics 174: 2255–2257. doi: 10.1534/genetics.106.063461 PMID: 17057238

102. Starz-Gaiano M, Cho NK, Forbes A, Lehmann R (2001) Spatially restricted activity of a Drosophila lipid phosphatase guides migrating germ cells. Development 128: 983–991. PMID: 11222152

103. St Pierre SE, Ponting L, Stefancsik R, McQuilton P, FlyBase C (2014) FlyBase 102–advanced approaches to interrogating FlyBase. Nucleic Acids Res 42: D780–788. doi: 10.1093/nar/gkt1092 PMID: 24234449

104. Li-Kroeger D, Witt LM, Grimes HL, Cook TA, Gebelein B (2008) Hox and senseless antagonism functions as a molecular switch to regulate EGF secretion in the Drosophila PNS. Dev Cell 15: 298–308. doi: 10.1016/j.devcel.2008.06.001 PMID: 18694568

105. Lohmann I, McGinnis N, Bodmer M, McGinnis W (2002) The Drosophila Hox gene deformed sculpts head morphology via direct regulation of the apoptosis activator reaper. Cell 110: 457–466. PMID: 12202035

106. Ohshiro T, Saigo K (1997) Transcriptional regulation of breathless FGF receptor gene by binding of TRACHEALESS/dARNT heterodimers to three central midline elements in Drosophila developing trachea. Development 124: 3975–3986. PMID: 9374395

107. Barrio R, de Celis JF, Bolshakov S, Kafatos FC (1999) Identification of regulatory regions driving the expression of the Drosophila spalt complex at different developmental stages. Dev Biol 215: 33–47. PMID: 10525348

108. Hosono C, Takaira K, Matsuda R, Saigo K (2003) Functional subdivision of trunk visceral mesoderm parasegments in Drosophila is required for gut and trachea development. Development 130: 439–449. PMID: 12490551

109. Bradley PL, Andrew DJ (2001) ribbon encodes a novel BTB/POZ protein required for directed cell migration in Drosophila melanogaster. Development 128: 3001–3015. PMID: 11532922

110. Inbal A, Volk T, Salzberg A (2004) Recruitment of ectodermal attachment cells via an EGFR-dependent mechanism during the organogenesis of Drosophila proprioceptors. Dev Cell 7: 241–250. PMID: 15296720

111. Skeath JB (1998) The Drosophila EGF receptor controls the formation and specification of neuroblasts along the dorsal-ventral axis of the Drosophila embryo. Development 125: 3301–3312. PMID: 9693134

112. Kumar JP, Tio M, Hsiung F, Akopyan S, Gabay L, et al. (1998) Dissecting the roles of the Drosophila EGF receptor in eye development and MAP kinase activation. Development 125: 3875–3885. PMID: 9729495

113. Hopmann R, Duncan D, Duncan I (1995) Transvection in the iab-5,6,7 region of the bithorax complex of Drosophila: homology independent interactions in trans. Genetics 139: 815–833. PMID: 7713434

114. Perrimon N, Noll E, McCall K, Brand A (1991) Generating lineage-specific markers to study Drosophila development. Dev Genet 12: 238–252. PMID: 1651183

115. Estacio-Gomez A, Moris-Sanz M, Schafer AK, Perea D, Herrero P, et al. (2013) Bithorax-complex genes sculpt the pattern of leucokinergic neurons in the Drosophila central nervous system. Development 140: 2139–2148. doi: 10.1242/dev.090423 PMID: 23633511

116. Urbach R, Technau GM (2003) Molecular markers for identified neuroblasts in the developing brain of Drosophila. Development 130: 3621–3637. PMID: 12835380

117. Lee JJ, von Kessler DP, Parks S, Beachy PA (1992) Secretion and localized transcription suggest a role in positional signaling for products of the segmentation gene hedgehog. Cell 71: 33–50. PMID: 1394430

118. Patel NH (1994) Imaging neuronal subsets and other cell types in whole-mount Drosophila embryos and larvae using antibody probes. Methods Cell Biol 44: 445–487. PMID: 7707967

119. Campos-Ortega JA, Hartenstein V (1997) The embryonic development of Drosophila melanogaster. Berlin; New York: Springer. xvii, 405 p. p.

120. White RA, Wilcox M (1984) Protein products of the bithorax complex in Drosophila. Cell 39: 163–171. PMID: 6091908

121. Kosman D, Small S, Reinitz J (1998) Rapid preparation of a panel of polyclonal antibodies to Drosophila segmentation proteins. Dev Genes Evol 208: 290–294. PMID: 9683745

122. Xie B, Charlton-Perkins M, McDonald E, Gebelein B, Cook T (2007) Senseless functions as a molecular switch for color photoreceptor differentiation in Drosophila. Development 134: 4243–4253. PMID: 17978002

123. Henderson KD, Isaac DD, Andrew DJ (1999) Cell fate specification in the Drosophila salivary gland: the integration of homeotic gene function with the DPP signaling cascade. Dev Biol 205: 10–21. PMID: 9882494

124. Celniker SE, Keelan DJ, Lewis EB (1989) The molecular genetics of the bithorax complex of Drosophila: characterization of the products of the Abdominal-B domain. Genes Dev 3: 1424–1436. PMID: 2575066

125. Blochlinger K, Bodmer R, Jan LY, Jan YN (1990) Patterns of expression of cut, a protein required for external sensory organ development in wild-type and cut mutant Drosophila embryos. Genes Dev 4: 1322–1331. PMID: 1977661

126. Yip ML, Lamka ML, Lipshitz HD (1997) Control of germ-band retraction in Drosophila by the zinc-finger protein HINDSIGHT. Development 124: 2129–2141. PMID: 9187140

127. Sampedro J, Guerrero I (1991) Unrestricted expression of the Drosophila gene patched allows a normal segment polarity. Nature 353: 187–190. PMID: 1653907

128. Jeon M, Zinn K (2009) Receptor tyrosine phosphatases control tracheal tube geometries through negative regulation of Egfr signaling. Development 136: 3121–3129. doi: 10.1242/dev.033597 PMID: 19675131

129. Goto S, Hayashi S (1997) Specification of the embryonic limb primordium by graded activity of Decapentaplegic. Development 124: 125–132. PMID: 9006073

130. Merabet S, Ebner A, Affolter M (2005) The Drosophila Extradenticle and Homothorax selector proteins control branchless/FGF expression in mesodermal bridge-cells. EMBO Rep 6: 762–768. doi: 10.1038/sj.embor.7400462 PMID: 16007069